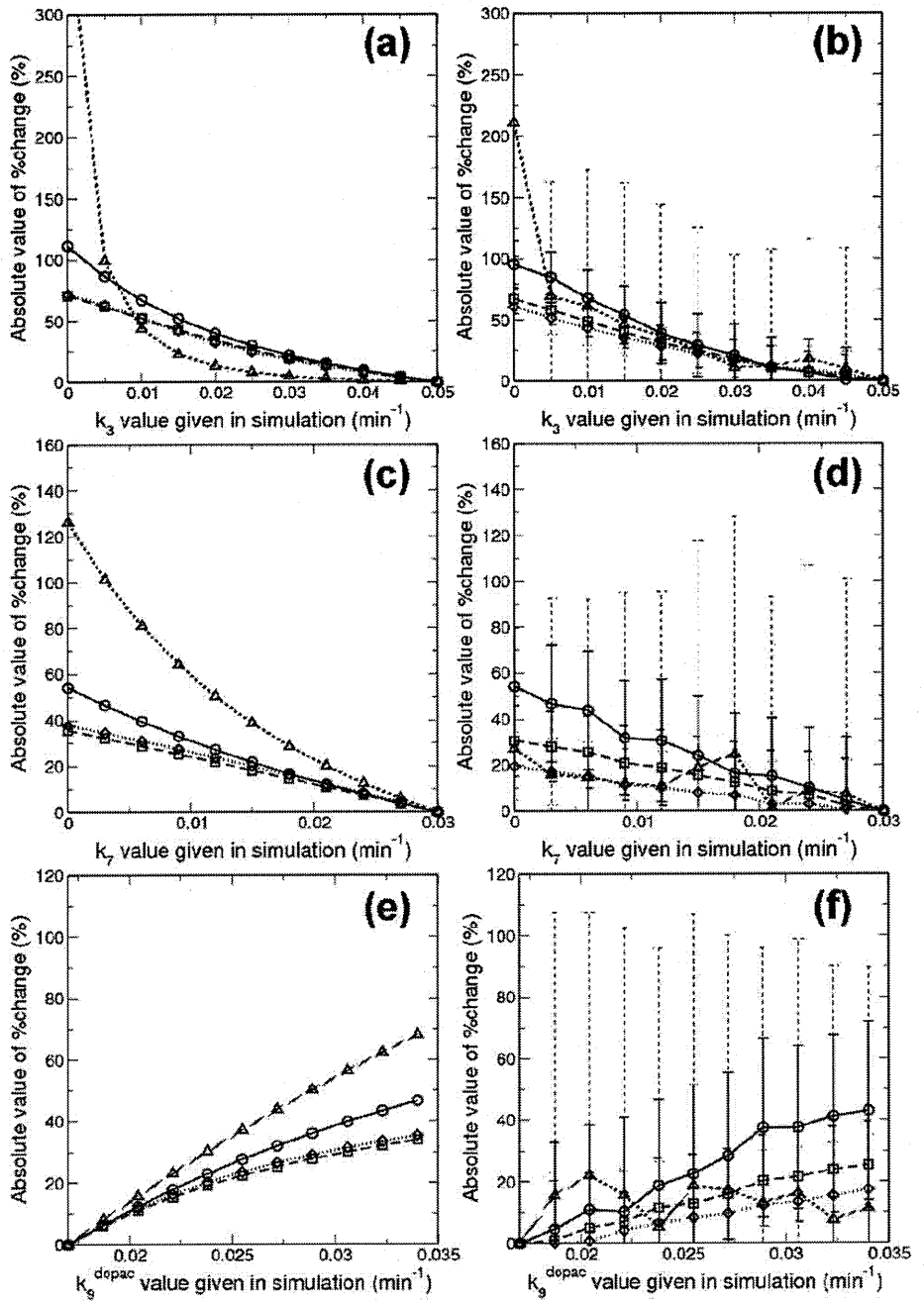

Fig. 5. Trends of percent change in the case of altering k_3 [upper row: (a), (b)], k_7 [middle row: (c), (d)], or k_9^{dopac} [bottom row: (e), (f)]. Noise free or noise added TACs were shown in left column [(a), (c), and (e)] or right column [(b), (d), and (f)], respectively. Legends: circles and solid lines: K_i (Gjedde-Patlak), squares and roughly dashed lines: V_T (Logan), diamonds and dotted lines: V_T (Kumakura), triangle and fine dashed lines: k_{loss} (Kumakura).

tor kinetic study (Kawatsu et al., 2002; Logan et al., 1990) and Kumakura method, which is proposed by Kumakura et al. (Kumakura et al., 2006). In noise-free simulations, k_{loss} estimated by Kumakura method showed the most sensitive to changes in k_7 and k_9^{dopac} among the conventional macro parameters, which suggests that k_{loss} is sensitive to the changes in dopamine storage and metabolism. This finding is in agreement with previous clinical studies (Kumakura et al., 2005, 2006) that show that among the macro parameters estimated by three conventional methods, k_{loss} was differentiated most clearly.

The interpretation of k_{loss} is that it represents the net diffusion of acidic metabolites of FDA, FDOPAC, and FHVA, from brain tissue (Holden et al., 1997; Kumakura et al., 2006; Sossi et al., 2001). Consistent with the definition of k_{loss}, is that it correlated well with the parameter of k_7 and k_9^{dopac} (Ishikawa et al., 1996; Ito et al., 2002; Kumakura et al., 2004; Martin et al., 1989; McGowan et al., 2004; Morrish et al., 1995; Piccini et al., 2005), which are related to washout of FDA and its metabolites from dopaminergic nerve as shown in Figure 2.

In multilinear fitting by Kumakura method, better correlation was observed relative to Patlak or Logan method even if noise were added to the simulated TACs. However, noise in C_{PET} heavily influenced the estimation of k_{loss} and resulted that k_{loss} estimated can not detect the changes in dopamine storage and metabolism significantly. By Kumakura et al., the overestimation of the voxel-wise estimates of k_{loss} was reported (Kumakura et al., 2006). These results and findings suggest voxel-wise estimation may not be optimum for k_{loss} estimation. Note that the voxel-noise was estimated empirically in our simulation. The noise level heavily depends on experimental conditions. For example, we acquired PET data in 2D mode and, the noise level is significantly reduced if we acquired PET data in 3D mode.

The bias of k_{loss} caused by noise can be suppressed by the rearrangement of multilinear equation in Kumakura method (Kumakura et al., 2010a), as described in Appendix. By the rearrangement of Kumakura method, the k_{loss} values were close to ones estimated from noise-free data (see Fig. 6).

K_i and V_T values changed more sensitively than k_{loss} when k_3 was altered between 0.0100 and 0.0500 min^{-1}. And, the changes in both noise added cases were significant. These results suggest that K_i and V_T can detect the changes in DDC activity more sensitively as compared with k_{loss}. However, k_{loss} was increased dramatically in the case that k_3 was reduced extremely (see upper row in Fig. 5) because k_{loss} approached to the [^{18}F]FDOPA efflux (k_2).

Our simulation with noise showed the robustness of the sensitivity of K_i and V_T to the changes in dopamine pathway, suggesting that K_i and V_T may be suitable for voxel-wise estimation in evaluation of DDC activity, dopamine storage, and metabolism with severe noise in PET data. However, by the procedure such as the rearrangement of Kumakura method, the sensitivity of k_{loss} in noisy case can be improved. This finding suggests k_{loss} may be potentially useful for voxel-wise estimation if the voxel-noise are suppressed.

Gjedde-Patlak analysis has been widely applied in the estimation of the net influx of [^{18}F]FDOPA or DDC activity from [^{18}F]FDOPA PET data (Bouilleret et al., 2005; Cheesman et al., 2005; Cumming and Gjedde, 1998; de la Fuente-Fernandez et al., 2000; Hilker et al., 2005; Ishikawa et al., 1996; Ito et al., 2002; Kumakura et al., 2004; Martin et al., 1989; McGowan et al., 2004; Morrish et al., 1995; Piccini et al., 2005). Linear regression in Gjedde-Patlak analysis, which uses only plasma activity data (C_a^D, see Eq. 3) as independent variables, is robust to the noise in PET data. In the present study, higher sensitivity of K_i to the reduction of DDC activity was suggested. Thus, Gjedde-Patlak analysis is adequate for the estimation of DDC activity.

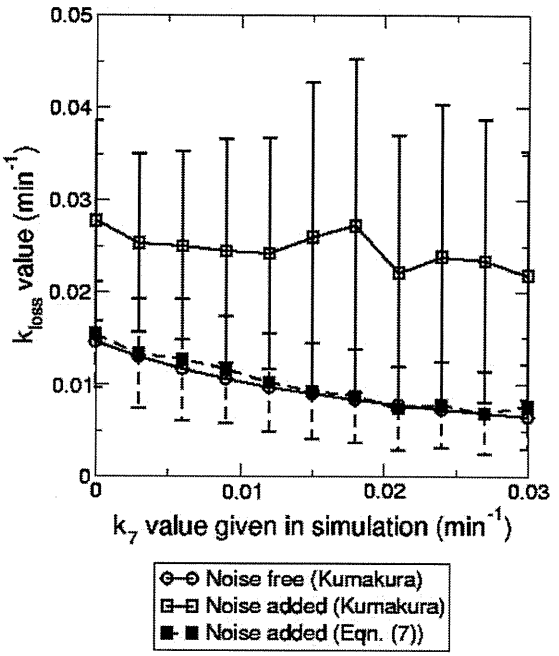

Fig. 6. Comparison trends of estimated k_{loss} between Kumakura method and Eq. 7. By Eq. 7, the bias of k_{loss} was suppressed.

Striatal [^{18}F]FDOPA kinetic is considered as irreversible and Gjedde-Patlak analysis has been applied most popularly in [^{18}F]FDOPA studies (Bouilleret et al., 2005; Cheesman et al., 2005; Cumming and Gjedde, 1998; de la Fuente-Fernandez et al., 2000; Hilker et al., 2005; Ishikawa et al., 1996; Ito et al., 2002; Kumakura et al., 2004; Martin et al., 1989; McGowan et al., 2004; Morrish et al., 1995; Piccini et al., 2005). However, reversible kinetics of [^{18}F]FDOPA was reported in the case of long dynamic PET scan (Holden et al., 1997; Sossi et al., 2001, 2002) and the case that OMFD component was corrected mathematically (Kumakura et al., 2005). Some investigators applied the graphical methods, which assumes the reversible tracer kinetics, for estimations of dopamine turnover and storage capacity (Holden et al., 1997; Kawatsu et al., 2002; Kumakura et al., 2005, 2006; Sossi et al., 2001, 2002). We examined

Logan and Kumakura method as methods for reversible kinetics in this study.

Our simulation model is based on the known dopamine pathway. Several compartment models have been proposed for [^{18}F]FDOPA (Huang et al., 1991; Kuwabara et al., 1993; Wahl and Nahmias, 1996). Deep et al. showed that a model that includes vesicular storage of [^{18}F]FDA, as well as metabolism to [^{18}F]FDOPAC and [^{18}F]FHVA was biologically accurate, based on the agreement between simulated and measured fraction of [^{18}F]FDOPA and its labeled metabolites in rat brain (Deep et al., 1997). A similar model that features both a slow clearing component (vesicular storage) and a fast clearing component ([^{18}F]FDOPA metabolism), and was found to be consistent with the fraction of [^{18}F]FDOPA, [^{18}F]FDOPAC, [^{18}F]FHVA, and [^{18}F]FDA measured in primate (Endres et al., 2004). The DF model used in this study was adapted from the models described above, and those models can be represented by uniting multiple compartments in the DF model. Note that the DF model is quite detailed, and here it is applied to simulate changes in several underlying processes that affect the tracer accumulation in [^{18}F]FDOPA PET studies. Although it is instructive to apply the model for simulations to improve the physiological interpretation of the kinetic macro parameters, the complexity of the DF model makes it unsuitable as a means for parameter estimation.

We simulated TACs that reflect known pathophysiological changes in Parkinson's disease, including the reduction of DDC activity, reduction of dopamine storage in the vesicle, and upregulation of dopamine turnover. Recently, Kumakura et al. suggested that dopamine storage capacity in the Parkinsonian brain is more impaired than is the net FDOPA influx (Kumakura et al., 2006). Chen et al. showed that the binding potential (BP) of [^{11}C]DTBZ, the radiotracer for VMAT2, decreased in a low-dose MPTP monkey and this decrease preceded changes in BP of [^{11}C]raclopride for D2-dopamine receptor and [^{11}C]WIN 35,428 for DAT (Chen et al., 2008). These findings suggest that the reduction of dopamine storage capacity in the vesicle may be a key event in the early phase of Parkinson's disease. According to these findings, and the results in this study, we propose that k_{loss} may be a useful index for early diagnosis of Parkinson's disease.

The upregulation of metabolism to HVA has been also observed in Parkinson's disease (Bernheimer et al., 1973; Hornykiewicz and Kish, 1987). We simulated the TACs with increasing k_9^{hva}, however, it made only a little differences in simulated TACs (data not shown). That suggests that the clearance of [^{18}F]FDA predominantly reflects the clearance of [^{18}F]FDOPAC. As [^{18}F]FDOPAC can clear via two pathways, that is, diffusion into CSF or metabolism to [^{18}F]FHVA, altering the clearance rate of [^{18}F]FHVA alone has minimal effect on the net clearance of [^{18}F]FDA.

In the present simulation, we generated a standard TAC to represent a normal TAC in monkey striatum. The interspecies difference between monkey and human should be considered to better interpret the sensitivity to detect changes in a patient with Parkinson's disease. For example, the clearance of [^{18}F]FDOPA in the plasma of monkey is faster than that in human (Melega et al., 1990). However, estimated k_{loss} values and its trends were close to the ones of normal human control and the patients with Parkinson's disease, resulted in previous human [^{18}F]FDOPA PET study (Kumakura et al., 2006).

We have considered the case of altering only one rate constant in each simulation. However, it is likely that DDC activity, dopamine storage, and metabolism will all be affected in patients with Parkinson's disease. It is necessary to simulate TACs with alteration of the parameters k_3, k_7, and k_9^{dopac} simultaneously for more practical evaluation. To further support our claim in this simulation study, [^{18}F]FDOPA PET experiments using Parkinsonian model animals would be interesting. However, it is clearly out of the scope of the present study.

The DF model could be applied to other physiological and pathological changes that are known to occur in the dopamine system. For example, the reduction of MAO activity in the brain of smokers has been reported (Fowler et al., 1996). For the patients with schizophrenia, the upregulation of DDC activity has been reported (Reith et al., 1994). Moreover, dysfunction of dopamine nerve in the basal ganglia of patients with other neurological disorders, such as epilepsy (Biraben et al., 2004; Bouilleret et al., 2005) and attention deficit hyperactivity disorder (ADHD) (Ludolph et al., 2008), have been reported.

CONCLUSION

For comparison of sensitivity of macro parameters estimated by conventional analyses to changes in DDC activity, dopamine storage and metabolism, we introduced a compartmental model that describes the detailed dopamine pathway (DF model) for simulating striatal TACs as observed in [^{18}F]FDOPA PET study. The present simulation demonstrated that k_{loss} by Kumakura method is relatively sensitive to the reduction of dopamine storage, and acceleration of dopamine metabolism from FDA to FDOPAC, whereas K_i and V_T can detect the reduction of DDC activity. Simulation with the DF model may help in the development of strategies to evaluate [^{18}F]FDOPA PET studies to optimize sensitivity to physiological changes that may occur in Parkinson's disease and the other neurological disorders.

REFERENCES

Bernheimer H, Birkmayer W, Hornykiewicz O, Jellinger K, Seitelberger F. 1973. Brain dopamine and the syndromes of Parkinson and Huntington. Clinical, morphological and neurochemical correlations. J Neurol Sci 20:415–455.

Biraben A, Semah F, Ribeiro M-J, Douaud G, Remy P, Depaulis A. 2004. PET evidence for a role of the basal ganglia in patients with ring chromosome 20 epilepsy. Neurology 63:73–77.

Borght TMV, Sima AA, Kilbourn MR, Desmond TJ, Kuhl DE, Frey KA. 1995. [3H]methoxytetrabenazine: A high specific activity ligand for estimating monoaminergic neuronal integrity. Neuroscience 68:955–962.

Bouilleret V, Semah F, Biraben A, Taussig D, Chassoux F, Syrota A, Ribeiro MJ. 2005. Involvement of the basal ganglia in refractory epilepsy: An 18F-fluoro-L-DOPA PET study using 2 methods of analysis. J Nucl Med 46:540–547.

Brooks D. 2004. Neuroimaging in Parkinson's disease. NeuroRx 1:243–254.

Chan GL, Doudet DJ, Dobko T, Hewitt KA, Schofield P, Pate BD, Ruth TJ. 1995. Routes of administration and effect of carbidopa pretreatment on 6-[18F]-fluoro-L-dopa/PET scans in non-human primates. Life Sci 56:1759–1766.

Cheesman AL, Barker RA, Lewis SJG, Robbins TW, Owen AM, Brooks DJ. 2005. Lateralisation of striatal function: Evidence from [18F]-dopa PET in Parkinson's disease. J Neurol Neurosurg Psychiatr 76:1204–1210.

Chen MK, Kuwabara H, Zhou Y, Adams RJ, Brasic JR, McGlothan JL, Verina T, Burton NC, Alexander M, Kumar A, Wong DF, Guilarte TR. 2008. VMAT2 and dopamine neuron loss in a primate model of Parkinson's disease. J Neurochem 105:78–90.

Cooper JR, Broom FE, Roth RH. 2003. The biochemical basis of neuropharmacology. Oxford University Press, USA. p197–234.

Cumming P, Boyes BE, Martin WRW, Adam M, Grierson J, Ruth T, McGeer EG. 1987. The metabolism of [18F]6-fluoro-L-3,4-dihydroxyphenylalanine in the hooded rat. J Neurochem 48:601–608.

Cumming P, Gjedde A. 1998. Compartmental analysis of dopa decarboxylation in living brain from dynamic positron emission tomograms. Synapse 29:37–61.

Cumming P, Kuwabara H, Gjedde A. 1994. A kinetic analysis of 6-[18F]fluoro-L-dihydroxyphenylalanine metabolism in the rat. J Neurochem 63:1675–1682.

Cumming P, Yokoi F, Chen A, Deep P, Dagher A, Reutens D, Kapczinski F, Wong DF, Gjedde A. 1999. Pharmacokinetics of radiotracers in human plasma during positron emission tomography. Synapse 34:124–134.

de la Fuente-Fernandez R, Pal PK, Vingerhoets FJ, Kishore A, Schulzer M, Mak EK, Ruth TJ, Snow BJ, Calne DB, Stoessl AJ. 2000. Evidence for impaired presynaptic dopamine function in parkinsonian patients with motor fluctuations. J Neural Transm 107:49–57.

Deep P, Gjedde A, Cumming P. 1997. On the accuracy of an [18F]FDOPA compartmental model: Evidence for vesicular storage of [18F]fluorodopamine in vivo. J Neurosci Methods 76:157–165.

Doudet DJ, McLellan CA, Carson R, Adams HR, Miyake H, Aigner TG, Finn RT, Cohen RM. 1991. Distribution and kinetics of 3-*O*-methyl-6-[18F]fluoro-L-dopa in the rhesus monkey brain. J Cereb Blood Flow Metab 11:726–734.

Endres CJ, DeJesus OT, Uno H, Doudet DJ, Nickles RJ, Holden JE. 2004. Time profile of cerebral [18F]6-fluoro-L-dopa metabolites in nonhuman primate: Implications for the kinetics of therapeutic L-dopa. Front Biosci 9:505–512.

Firnau G, Sood S, Chirakal R, Nahmias C, Garnett ES. 1987. Cerebral metabolism of 6-[18f]fluoro-L-3,4-dihydroxyphenylalanine in the primate. J Neurochem 48:1077–1082.

Fowler J, Logan J, Volkow N, Wang G, MacGregor R, Ding Y. 2002. Monoamine oxidase: Radiotracer development and human studies. Methods 27:263–277.

Fowler JS, Volkow ND, Wang GJ, Pappas N, Logan J, MacGregor R, Alexoff D, Shea C, Schlyer D, Wolf AP, Warner D, Zezulkova I, Cilento R. 1996. Inhibition of monoamine oxidase B in the brains of smokers. Nature 379:733–736.

Frey KA, Koeppe RA, Kilbourn MR, Borght TMV, Albin RL, Gilman S, Kuhl DE. 1996. Presynaptic monoaminergic vesicles in Parkinson's disease and normal aging. Ann Neurol 40:873–884.

Gjedde A. 1981. High- and low-affinity transport of D-glucose from blood to brain. J Neurochem 36:1463–1471.

Gjedde A. 1982. Calculation of cerebral glucose phosphorylation from brain uptake of glucose analogs in vivo: A re-examination. Brain Res 257:237–274.

Gjedde A, Leger GC, Cumming P, Yasuhara Y, Evans AC, Guttman M, Kuwabara H. 1993. Striatal L-dopa decarboxylase activity in Parkinson's disease in vivo: Implications for the regulation of dopamine synthesis. J Neurochem 61:1538–1541.

Herzog H, Tellmann L, Hocke C, Pietrzyk U, Casey ME, Kuwert T. 2004. NEMA NU2-2001 guided performance evaluation of four Siemens ECAT PET scanners. IEEE Trans Nucl Sci 51:2662–2669.

Hilker R, Thomas AV, Klein JC, Weisenbach S, Kalbe E, Burghaus L, Jacobs AH, Herholz K, Heiss WD. 2005. Dementia in Parkinson disease: Functional imaging of cholinergic and dopaminergic pathways. Neurology 65:1716–1722.

Holden JE, Doudet D, Endres CJ, Chan GL-Y, Morrison KS, Vingerhoets FJG, Snow BJ, Pate BD, Sossi V, Buckley KR, Ruth TJ. 1997. Graphical analysis of 6-fluoro-L-dopa trapping: Effect of inhibition of catechol-*O*-methyltransferase. J Nucl Med 38:1568–1574.

Hornykiewicz O, Kish SJ. 1987. Biochemical pathophysiology of Parkinson's disease. Adv Neurol 45:19–34.

Huang S, Yu D, Barrio J, Grafton S, Melega W, Hoffman J, Satyamurthy N, Mazziotta J, Phelps M. 1991. Kinetics and modeling of L-6-[18F]fluoro-dopa in human positron emission tomographic studies. J Cereb Blood Flow Metab 11:898–913.

Ishikawa T, Dhawan V, Chaly T, Margouleff C, Robeson W, Dahl JR, Mandel F, Spetsieris P, Eidelberg D. 1996. Clinical significance of striatal DOPA decarboxylase activity in Parkinson's disease. J Nucl Med 37:216–222.

Ito K, Nagano-Saito A, Kato T, Arahata Y, Nakamura A, Kawasumi Y, Hatano K, Abe Y, Yamada T, Kachi T, Brooks DJ. 2002. Striatal and extrastriatal dysfunction in Parkinson's disease with dementia: A 6-[18F]fluoro-L-dopa PET study. Brain 125:1358–1365.

Kawatsu S, Kato T, Nagano-Saito A, Hatano K, Ito K, Ishigaki T. 2002. New insight into the analysis of 6-[18F]fluoro-L-DOPA PET dynamic data in brain tissue without an irreversible compartment: Comparative study of the Patlak and Logan analyses. Radiat Med 21:47–54.

Kudomi N, Choi E, yamamoto S, Watabe H, Kim KM, Shidahara M, Ogawa M, Teramoto N, Sakamoto E, Iida H. 2003. Development of a GSO detector assembly for a continuous blood sampling system. IEEE Trans Nucl Sci 50:70–73.

Kumakura Y, Danielsen EH, Reilhac A, Gjedde A, Cumming P. 2004. Levodopa effect on [18F]fluorodopa influx to brain: Normal volunteers and patients with Parkinson's disease. Acta Neurol Scand 110:188–195.

Kumakura Y, Vernaleken I, Grunder G, Bartenstein P, Gjedde A, Cumming P. 2005. PET studies of net blood-brain clearance of FDOPA to human brain: Age-dependent decline of [18F]fluorodopamine storage capacity. J Cereb Blood Flow Metab 25:807–819.

Kumakura Y, Gjedde A, Danielsen EH, Christensen S, Cumming P. 2006. Dopamine storage capacity in caudate and putamen of patients with early Parkinson's disease: Correlation with asymmetry of motor symptoms. J Cereb Blood Flow Metab 26:358–370.

Kumakura Y, Cumming P, Vernaleken I, Buchholz HG, Siessmeier T, Heinz A, Kienast T, Bartenstein P, Grunder G. 2007. Elevated [18F]fluorodopamine turnover in brain of patients with schizophrenia: An [18F]fluorodopa/positron emission tomography study. J Neurosci 27:8080–8087.

Kumakura Y, Danielsen EH, Gjedde A, Vernaleken I, Buchholz H-G, Heinz A, Gränder G, Bartenstein P, Cumming P. 2010a. Elevated [(18)F]FDOPA utilization in the periaqueductal gray and medial nucleus accumbens of patients with early Parkinson's disease. Neuroimage 49:2933–2939.

Kumakura Y, Vernaleken I, Buchholz H-G, Borghammer P, Danielsen E, Grnder G, Heinz A, Bartenstein P, Cumming P. 2010b. Age-dependent decline of steady state dopamine storage capacity of human brain: An FDOPA PET study. Neurobiol Aging 31:447–463.

Kuwabara H, Cumming P, Reith J, LY¥eg G, Diksic M, Evans A, Gjedde A. 1993. Human striatal L-dopa decarboxylase activity estimated in vivo using 6-[18F]fluoro-dopa and positron emission tomography: Error analysis and application to normal subjects. J Cereb Blood Flow Metab 13:43–56.

Lee CS, Samii A, Sossi V, Ruth TJ, Schulzer M, Holden JE, Wudel J, Pal PK, de la Fuente-Fernandez R, Calne DB, Stoessl AJ. 2000. In vivo positron emission tomographic evidence for compensatory changes in presynaptic dopaminergic nerve terminals in Parkinson's disease. Ann Neurol 47:493–503.

Lloyd K, Hornykiewicz O. 1970. Parkinson's disease: Activity of L-dopa decarboxylase in discrete brain regions. Science 170:1212–1213.

Logan J, Fowler JS, Volkow ND, Wolf AP, Dewey SL, Schlyer DJ, MacGregor RR, Hitzemann R, Bendriem B, Gatley SJ. 1990. Graphical analysis of reversible radioligand binding from time-ac-

tivity measurements applied to [N-^{11}C-methyl]-(-)-cocaine PET studies in human subjects. J Cereb Blood Flow Metab 10:740–747.
Ludolph AG, Kassubek J, Schmeck K, Glaser C, Wunderlich A, Buck AK, Reske SN, Fegert JM, Mottaghy FM. 2008. Dopaminergic dysfunction in attention deficit hyperactivity disorder (ADHD), differences between pharmacologically treated and never treated young adults: A 3,4-dihdroxy-6-[^{18}F]fluorophenyl-L-alanine PET study. Neuroimage 41:718–727.
Martin WR, Palmer MR, Patlak CS, Calne DB. 1989. Nigrostriatal function in humans studied with positron emission tomography. Ann Neurol 26:535–542.
Matsubara K, Watabe H, Hayashi T, Minato K, Iida H. 2010. Evaluation of bias of the influx constant estimated by Patlak analysis for [^{18}F]FDOPA PET: Influence of metabolites for [^{18}F]FDOPA. Seitai-Ikougaku 48:66–74.
McGowan S, Lawrence AD, Sales T, Quested D, Grasby P. 2004. Presynaptic dopaminergic dysfunction in schizophrenia: A positron emission tomographic [^{18}F]fluorodopa study. Arch Gen Psychiatry 61:134–142.
Melega WP, Hoffman JM, Luxen A, Nissenson CHK, Phelps ME, Barrio JR. 1990. The effects of carbidopa on the metabolism of 6-[^{18}F]fluoro-L-dopa in rats, monkeys and humans. Life Sci 47:149–157.
Morrish PK, Sawle GV, Brooks DJ. 1995. Clinical and [^{18}F] dopa PET findings in early Parkinson's disease. J Neurol Neurosurg Psychiatr 59:597–600.
Pajevic S, Daube-Witherspoon ME, Bacharach SL, Carson RE. 1998. Noise characteristics of 3-D and 2-D PET images. IEEE Trans Med Imaging 17:9–23.
Patlak CS, Blasberg RG. 1985. Graphical evaluation of blood-to-brain transfer constants from multiple-time uptake data. Generalizations. J Cereb Blood Flow Metab 5:584–590.
Patlak CS, Blasberg RG, Fenstermacher JD. 1983. Graphical evaluation of blood-to-brain transfer constants from multiple-time uptake data. J Cereb Blood Flow Metab 3:1–7.
Piccini P, Pavese N, Hagell P, Reimer J, Bjorklund A, Oertel WH, Quinn NP, Brooks DJ, Lindvall O. 2005. Factors affecting the clinical outcome after neural transplantation in Parkinson's disease. Brain 128:2977–2986.
Pifl C, Hornykiewicz O. 2006. Dopamine turnover is upregulated in the caudate/putamen of asymptomatic MPTP-treated rhesus monkeys. Neurochem Int 49:519–524.
Reith J, Benkelfat C, Sherwin A, Yasuhara Y, Kuwabara H, Andermann F, Bachneff S, Cumming P, Diksic M, Dyve SE, Etienne P, Evans AC, Lal S, Shevell M, Savard G, Wong DF, Chouinard G, Gjedde A. 1994. Elevated dopa decarboxylase activity in living brain of patients with psychosis. Proc Natl Acad Sci USA 91:11651–11654.
Shidahara M, Watabe H, Kim KM, Kudomi N, Ito H, Iida H. 2008. Optimal scan time of oxygen-15-labeled gas inhalation autoradiographic method for measurement of cerebral oxygen extraction fraction and cerebral oxygen metabolic rate. Ann Nucl Med 22:667–675.
Sossi V, Doudet DJ, Holden JE. 2001. A reversible tracer analysis approach to the study of effective dopamine turnover. J Cereb Blood Flow Metab 21:469–476.
Sossi V, de La Fuente-Fernandez R, Holden JE, Doudet DJ, McKenzie J, Stoessl AJ, Ruth TJ. 2002. Increase in dopamine turnover occurs early in Parkinson's disease: Evidence from a new modeling approach to PET ^{18}F-fluorodopa data. J Cereb Blood Flow Metab 22:232–239.
Sossi V, Holden J, de la Fuente-Fernandez R, Ruth T, Stoessl A. 2003. Effect of dopamine loss and the metabolite 3-*O*-methyl-[^{18}F]fluoro-dopa on the relation between the 18F-fluorodopa tissue input uptake rate constant Kocc and the [^{18}F]fluorodopa plasma input uptake rate constant Ki. J Cereb Blood Flow Metab 23:301–309.
Sossi V, de la Fuente-Fernandez R, Holden JE, Schulzer M, Ruth TJ, Stoessl J. 2004. Changes of dopamine turnover in the progression of Parkinson's disease as measured by positron emission tomography: Their relation to disease-compensatory mechanisms. J Cereb Blood Flow Metab 24:869–876.
Sossi V, de la Fuente-Fernandez R, Schulzer M, Troiano AR, Ruth TJ, Stoessl AJ. 2007. Dopamine transporter relation to dopamine turnover in Parkinson's disease: A positron emission tomography study. Ann Neurol 62:468–474.
Stark H, Woods J, Paul I, Hingorani R. 1981. Direct Fourier reconstruction in computer tomography. IEEE Trans Acoust Speech Signal Processing 29:237–245.
Takagi Y, Takahashi J, Saiki H, Morizane A, Hayashi T, Kishi Y, Fukuda H, Okamoto Y, Koyanagi M, Ideguchi M, Hayashi H, Imazato T, Kawasaki H, Suemori H, Omachi S, Iida H, Itoh N, Nakatsuji N, Sasai Y, Hashimoto N. 2005. Dopaminergic neurons generated from monkey embryonic stem cells function in a Parkinson primate model. J Clin Invest 115:102–109.
Takikawa S, Dhawan V, Chaly T, Robeson W, Dahl R, Zanzi I, Mandel F, Spetsieris P, Eidelberg D. 1994. Input functions for 6-[fluorine-18]fluorodopa quantitation in parkinsonism: Comparative studies and clinical correlations. J Nucl Med 35:955–963.
Wahl L, Nahmias C. 1996. Modeling of fluorine-18-6-fluoro-l-dopa in humans. J Nucl Med 37:432–437.
Watabe H, Endres CJ, Breier A, Schmall B, Eckelman WC, Carson RE. 2000. Measurement of dopamine release with continuous infusion of [^{11}C]raclopride: Optimization and signal-to-noise considerations. J Nucl Med 41:522–530.

APPENDIX: REARRANGED KUMAKURA METHOD

Generally, the noise in TAC can be reduced by the integral. Thus, the noise influences to k_{loss} can be reduced by transposition between C_{PET} and its integral in Eq. 5 as the following (Kumakura et al., 2010a):

$$\bar{C}_{\mathrm{PET}}(t) = V_{\mathrm{T}} \cdot k_{\mathrm{loss}} \cdot \int_0^t C_{\mathrm{a}}^{\mathrm{D}}(\tau)d\tau - k_{\mathrm{loss}} \cdot \int_0^t \bar{C}_{\mathrm{PET}}(\tau)d\tau + (V_{\mathrm{f}} + V_{\mathrm{b}}) \cdot C_{\mathrm{a}}^{\mathrm{D}}(t) \qquad (7)$$

This equation can directly and simply obtain k_{loss} from second term parameter estimated by multilinear fitting. It doesn't need additional procedure of estimated parameters, as reverse of second term parameter in Kumakura method.

International Journal of Pharmaceutics 404 (2011) 271–280

Contents lists available at ScienceDirect

International Journal of Pharmaceutics

journal homepage: www.elsevier.com/locate/ijpharm

Pharmaceutical Nanotechnology

Effects of organic solvents on drug incorporation into polymeric carriers and morphological analyses of drug-incorporated polymeric micelles

Yoshiko Harada[a], Tatsuhiro Yamamoto[b], Masaru Sakai[c], Toshiharu Saiki[c,d], Kumi Kawano[e], Yoshie Maitani[e], Masayuki Yokoyama[b,f,*]

[a] Japan Science and Technology Agency, ERATO, Takahara Soft Interfaces Project, CE80, Kyushu University, 744 Motooka, Nishi-ku, Fukuoka 819-0395, Japan
[b] Yokoyama Nanomedical Project, Kanagawa Academy of Science and Technology, KSP East 404, 3-2-1 Sakado, Takatsu-ku, Kawasaki 213-0012, Japan
[c] Near-Field Optics Group, Kanagawa Academy of Science and Technology, KSP East-409, 3-2-1 Sakado, Takatsu-ku, Kawasaki 213-0012, Japan
[d] Department of Electronics and Electrical Engineering, Faculty of Science and Technology, Keio University, 3-14-1 Hiyoshi, Kohoku-ku, Yokohama-shi, Kanagawa-ken 223-8522, Japan
[e] Institute of Medicinal Chemistry, Hoshi University, 2-4-41 Ebara, Shinagawa-ku, Tokyo 142-8501, Japan
[f] Medical Engineering Laboratory, Research Center for Medical Science, Jikei University School of Medicine, 3-25-8, Nishi-shinbashi, Minato-ku, Tokyo 105-8461 Japan

ARTICLE INFO

Article history:
Received 20 August 2010
Received in revised form 21 October 2010
Accepted 11 November 2010
Available online 18 November 2010

Keywords:
Polymeric micelle
Camptothecin
Incorporation
Inner core
Targeting
Morphology

ABSTRACT

We incorporated an anticancer agent, camptothecin (CPT), into polymeric micelle carriers by using two different solvents (TFE and chloroform) in the solvent-evaporation drug incorporation process. We observed significant differences in the drug-incorporation behaviors, in the morphologies of the incorporated drug and the polymeric micelles, and in the pharmacokinetic behaviors between the two solvents' cases. In particular, the CPT-incorporated polymeric micelles prepared with TFE as the incorporation solvent exhibited more stable circulation in blood than those prepared with chloroform. This contrast indicates a novel technological perspective regarding the drug incorporation into polymeric micelle carriers. Morphological analyses of the inner core have revealed the presence of the directed alignment of the CPT molecules and CPT crystals in the micelle inner core. This is the first report of the morphologies of the drug incorporated into the polymeric micelle inner cores. We believe these analyses are very important for further pharmaceutical developments of polymeric micelle drug-carrier systems.

1. Introduction

Polymeric micelles have attracted much attention as a nano-sized drug carrier in drug delivery systems (DDS) (Yokoyama, 2005; Aliabadi and Lavasanifar, 2006; Yokoyama, 2007). Polymeric micelles are macromolecular assemblies that, formed from block copolymers or graft copolymers, have a spherical inner core and an outer shell (Tuzar and Kratochvil, 1976,). Most typically, polymeric micelle drug carrier systems form from an AB type of block copolymer possessing a hydrophobic block and a hydrophilic block (Bader et al., 1984; Yokoyama et al., 1989). Hydrophobic drugs are physically incorporated into the micelles' hydrophobic inner cores by means of hydrophobic interactions (Kwon et al., 1994a; Yokoyama et al., 1994; Molavi et al., 2008; Shin et al., 2009). Owing to their advantages such as very small size in a range of 10–100 nm and high structural stability, polymeric micelle carriers have been actively applied to drug targeting (Yokoyama et al., 1991; Yokoyama, 2005; Aliabadi and Lavasanifar, 2006). In particular, polymeric micelle systems have achieved successful tumor targeting (Kwon et al., 1994b; Yokoyama et al., 1999; Nishiyama et al., 2003; Kawano et al., 2006) through the enhanced permeability and retention (EPR) effect (Matsumura and Maeda, 1986; Maeda et al., 1992), which enables nano-sized carriers to deliver anti-cancer drugs selectively to solid tumor sites. Presently, five clinical trials are underway for tumor targeting with polymeric micelle systems (Matsumura et al., 2004; Hamaguchi et al., 2005; Koizumi et al., 2006; Hamaguchi et al., 2007; Nakajima et al., 2008a,b).

Among the several types of nano-sized carrier systems including liposomes, nano-spheres, antibodies, and water-soluble synthetic polymers, the polymeric micelle has exhibited strong advantages in applications to hydrophobic low-molecular-weight drugs owing to the micelle's large drug-loading capacity and the micelle's ability to maintain the water solubility of the given carrier system. Previous studies of polymeric micelle drug-carrier systems have indicated that the stable incorporation of drugs into the hydrophobic inner cores is essential for successful in vivo targeting (Yokoyama et al., 1999; Yokoyama, 2005). If the stability is low, the drug is very rapidly released (within a range of only several minutes) from the carrier, resulting in unsuccessful targeting. Kwon et al. reported that extremely low diffusion constant

* Corresponding author. Tel.: +81 3 3433 1111x2336; fax: +81 3 3459 6005.
E-mail address: masajun2093ryo@jikei.ac.jp (M. Yokoyama).

0378-5173/$ – see front matter © 2010 Elsevier B.V. All rights reserved.
doi:10.1016/j.ijpharm.2010.11.016

values in a 10^{-19} to 10^{-20} cm^2/s order were necessary for stable drug incorporation because the size of micelle inner cores is very small, being approximately 10 nm in diameter (Forrest et al., 2006a,b). Yokoyama et al. reported that a slight change in the chemical structures of inner-core-forming hydrophobic polymer chains had substantial effects on incorporation stability (Yokoyama et al., 2004; Watanabe et al., 2006; Yamamoto et al., 2007). However, little is known about key factors for stable incorporation. Furthermore, physico-chemical characterizations of the incorporated drug molecules have never been conducted even though these characterizations would no double be useful both for the elucidation and the achievement of incorporation stability. These characterizations may concern, for example, types of drug distribution (uniformly distributed or localized at specific sites such as a boundary with an outer shell), aggregation status (the dispersed individual drug molecules or the aggregation of drug molecules into a cluster), and drug molecules' polarity (randomly directed drug molecules or molecules aligned to a specific direction owing to intermolecular interactions). Researchers have reported that two successful polymeric micelle systems physically incorporated drug molecules possessing planar chemical structures, doxorubicin (Yokoyama et al., 1991, 1999) and camptothecin (CPT) (Watanabe et al., 2006; Yamamoto et al., 2007). Doxorubicin possesses a planar anthracycline ring, and CPT molecules have a planar five-membered-ring structure. Planar molecules can exhibit strong polarity if they are aligned in one direction through their intermolecular associations. Therefore, the polarity of incorporated drug molecules is a candidate for determining factors that underlie stable incorporation.

In this paper, we carry out the first physico-chemical examination of the incorporated drug molecules inside micelle inner cores by means of fluorescence spectroscopy and AFM. Furthermore, we evaluate effects that solvents used in drug-incorporation procedures can have on both the morphologies of inner cores and the morphologies of micelle structures. Then, we compare two polymeric micelle formulations that are different from each other only in the solvent used in the drug incorporation process, while the other factors, drug molecules and block copolymer structures, are the same between the two formulations. We observed a substantial difference in pharmacokinetic behaviors. This indicates that solvents can be an important factor in successful drug incorporation through the control of morphologies, whether in relation to incorporated drugs or polymeric micelles.

2. Materials and methods

2.1. Materials

(s)-(+)-Camptothecin and 1,1,1-trifluoro-2-propanol were purchased from Sigma-Aldrich (Tokyo branch, Japan) and were used as received. Reagent-grade solvents, chloroform, 2,2,2-trifluoroethanol (TFE), tetrahydrofuran (THF), dimethylsulfoxide (DMSO), N,N-dimethylformamide (DMF), N,N-dimethylacetamide (DMAc), 1,4-dioxane, 1,1,1,3,3,3-hexafluoro isopropanol were purchased from Wako Chemicals (Tokyo, Japan) and were used as received. Poly(ethylene glycol)-b-poly(aspartic acid-co-benzyl aspartate) (PEG-P(Asp(Bzl 74))) was synthesized as previously reported (Opanasopit et al., 2004; Yokoyama et al., 2004; Yamamoto et al., 2007), and its chemical structure is shown in Fig. 1. The average molecular weight of PEG was 5200 (n = 118 in Fig. 1), and the average number of Asp units (m) was 27. The current study converted 74% of the aspartic-acid units into benzyl-aspartate units through an esterification reaction of poly(ethylene glycol)-b-poly(aspartic acid). Our group has investigated variations of this type of block polymer by, for example, changing the percentage of benzyl aspartate units or using hydrophobic ester groups

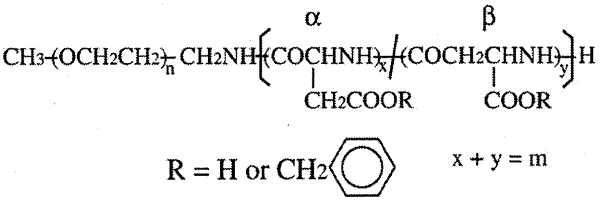

Fig. 1. Chemical structure of a block copolymer for micelle carriers.

other than benzyl ester, and so far PEG-P(Asp(Bzl 74) has worked well for our efforts to incorporate camptothecin into polymeric micelles (Yokoyama et al., 2004; Yamamoto et al., 2007) and to incorporate retinoids into polymeric micelles (Chansri et al., 2008; Okuda et al., 2008, 2009). The aspartate amide bond can be either α or β, and our group previously had reported that PEG-P(Asp(Bzl)) with all α aspartate amide bonds did not result in the formation of stable CPT-incorporated micelles. Therefore, in the current study, we used a polymer that has the aspartate amide bond with an α/β ratio of 1/3.

In some measurements, block copolymers possessing the same chain lengths and similar benzyl-esterification degrees (70% and 82%) were used.

2.2. Preparation of camptothecin-incorporated polymeric micelles

Camptothecin (CPT)-incorporated polymeric micelles were prepared through a solvent evaporation method (Yokoyama et al., 2004; Watanabe et al., 2006). In this method, 5 mg of PEG-P(Asp(Bzl 74)) and an appropriate amount of 1 mg/mL CPT solution (in TFE or chloroform) were mixed in a 9 mL glass vial, followed by evaporation of the solvent under a dry nitrogen-gas flow with stirring at 40–50 °C. After complete evaporation, a dried film was obtained. To this film was added 4 mL of water, and the mixture was sonicated with a probe type ultrasonication instrument (VCX-750 equipped with a 5 mm tapered micro tip, Sonics & Materials, Newtown, CT, USA). For removal of possible precipitates and large particles, the obtained solution was centrifuged at 10,000 rpm (12,000 × g) for 10 min by the use of a centrifuge Himac CR21G equipped with an R20A2 rotor (Hitachi Koki Co., Ltd., Tokyo, Japan) at 20 °C, and then was filtered through a 0.45 μm Millex-HV PVDF filter (Millipore Corp., Billerica, MA, USA), resulting in an aqueous solution of CPT-incorporated polymeric micelles. Polymeric micelles prepared by the use of TFE are denoted as "micelle A", and those prepared by the use of chloroform as "micelle B". A blank experiment was conducted in the absence of the block copolymer for estimating the amount of free CPT that would not be incorporated into polymeric micelles but that would be included in the solution. As the blank controls in which no polymer was used, CPT in a 1 mg/mL solution was added to an empty vial so that the total mass of CPT would be 0.5, 1.0, 2.0, or 5.0 mg, corresponding to 10, 20, 40, or 100 wt.% CPT with respect to polymers if they were present. The solvent was removed by evaporation, followed by an addition of water, sonication, centrifugation, and filtration according to the same approach as that adopted in the preparation of the CPT micelle solution. The concentration of CPT was measured with a UV–vis spectrometer. The procedure for UV–vis measurements is described in the UV–-vis spectroscopy Section 2.3.2.

2.3. Measurements

2.3.1. Dynamic light scattering (DLS)

Particle sizes of micelles were measured with a dynamic light scattering (DLS) instrument DLS-7000 (Otsuka Electronics, Tokyo,

Japan). The DLS samples were prepared by dilution of the micelle solutions with filtered Millipore water, while the polymer concentration was kept above the critical micelle concentration (CMC) reported in our previous paper (Yamamoto et al., 2007). The measurements were made at 25 °C, and scattering was observed at a 90° angle with respect to the incident beam. The Cumulant average particle size and particle size distribution from a non-negative least square method were determined by the use of software provided with the instrument. The DLS sample concentration was adjusted so that the scattering intensity would be within the measurable range, while the polymer concentration would be above its CMC.

2.3.2. UV–vis spectroscopy

The CPT concentrations of the micelle solutions were determined with a UV–vis spectrometer (Jasco V-550, JASCO Corp., Tokyo, Japan). The path length of the quartz cell was 1 cm. The scan range was 250–600 nm; the band width was set at 0.5 nm. CPT concentrations were calculated from an equation obtained from a calibration plot. Typically, a 150 μL sample aqueous solution, 150 μL water, and 2.7 mL DMSO were mixed to provide a 9:1 (vol./vol.) mixture of DMSO and water, and the peak top absorbance at 365 nm (A365) and the absorbance at 600 nm (A600) were recorded. The subtracted values (A365–A600) were used for the [CPT] determination. The CPT recovery in the drug-incorporation procedure was calculated through division of the micelle solution's "CPT amount" by the feed-added "CPT amount". When water was used in relation to the DMSO-water mixture as the solvent for UV–vis measurements, the dilution was 1/10 instead of 1/20.

We investigated the solubility of CPT in several organic solvents such as THF, DMF, and 1,4-dioxane, as well as in fluorinated solvents such as TFE and 1,1,1,3,3,3-hexafluoro isopropanol. CPT was dissolved in each solvent (up to 5 mg/mL), and absorbance at 600 nm was measured with a UV–vis spectrometer. We estimated the solubility of CPT in each solvent by measuring turbidity at 600 nm, because the CPT molecule has no absorption at 600 nm, and thus the absorbance recorded at this wavelength is caused by the light scattering of aggregated CPT.

2.3.3. Fluorescence spectroscopy

We measured polarization degrees of CPT molecules in the polymeric micelles by using a fluorescence-spectroscopy instrument (Jasco FP-6500, JASCO Corp., Tokyo, Japan) equipped with a polarization unit (JASCO Corp., Tokyo, Japan). Fluorescent spectra were recorded with excitation and emission at 351.5 nm and 433.0 nm, respectively. Band widths of excitation and emission were set at 10 nm and 3 nm, respectively. A fluorescence anisotropy (r) value was obtained by the formula $r = (I_{vv} - G \times I_{vh})/(I_{vv} + G \times I_{vh})$, where G is equivalent to I_{hv}/I_{hh}, where I_{vv} is equivalent to fluorescence intensity at vertical (excitation, Ex) and vertical (emission, Em) positions, where I_{vh} is equivalent to fluorescence intensity at vertical (Ex) and horizontal (Em) positions, where I_{hv} is equivalent to fluorescence intensity at horizontal (Ex) and vertical (Em) positions, and where I_{hh} is equivalent to fluorescence intensity at horizontal (Ex) and horizontal (Em) positions.

2.3.4. Polarized fluorescence microscopy

Polarized fluorescence microscopy, featuring a hand-made microscope, was carried out for a dried polymeric micelle sample on a quartz plate. An Ar-ion laser (351.1 nm; Innova 300, Coherent Inc., California, U.S.A.) with a polarization controller (SIGMA KOKI, Tokyo, Japan) was used for excitation, and a perpendicularly polarized component of the fluorescence signal was selectively observed with a supersensitive CCD camera (C4742-95ER, Hamamatsu Photonics, Shizuoka, Japan).

2.3.5. Atomic force microscopy (AFM)

For imaging by atomic force microscopy (AFM), micellar solutions were deposited on freshly cleaved mica, rinsed with water after a few minutes, and air (or nitrogen) dried; in this way, films were obtained. Height-contrast and phase-contrast images were obtained in air with an atomic force microscope MFP-3D (Asylum Research, Santa Barbara, CA, USA) in AC mode.

2.3.6. Determination of CPT concentrations in plasma

A CPT micelle solution in 0.9 wt.% NaCl was administered via the tail vein to male ddY mice (5 weeks old) at 2.5 mg CPT/kg. At 4 h after injection, blood was collected with a heparinized syringe, and the collected blood sample was centrifuged so that plasma could be obtained. The plasma was acidified with a 0.15 M phosphoric acid aqueous solution, and CPT was extracted with 4/1 (vol./vol.) chloroform/methanol. The extracted CPT was analyzed by the use of an HPLC system (LC-10AT, Shimadzu Corp., Kyoto, Japan) equipped with a Tosoh TSK-gel ODS-80Ts column (Tosoh, Corp., Tokyo, Japan), and a fluorescence detector set at $\lambda_{ex} = 369$ nm and $\lambda_{em} = 426$ nm. The mobile phase was a 23/77 vol./vol. mixture of acetonitrile/triethylamine acetate buffer (1.0% vol./vol., pH 5.5), and the flow rate of 1.0 mL/min was used.

2.3.7. Calculation of cohesion parameters

The partial cohesion parameters (δD, δP, and δH) for CPT and polymers were calculated from the molar volumes and the Hansen parameters listed in a reference (Hansen, C.M., 2007), and the total (Hildebrand) cohesion (solubility) parameter δt was obtained with the equation $\delta t = (\delta D^2 + \delta P^2 + \delta H^2)^{1/2}$. The parameters for the hydrophobic block, P(Asp(Bzl 74)), were calculated as molar-ratio-averages of the two repeating units Asp (26%) and Asp(Bzl) (74%).

3. Results

3.1. Preparation of CPT-incorporated polymeric micelles

We used block copolymer PEG-P(Asp(Bzl 74)) for the incorporation of camptothecin (CPT) into the polymeric micelle. Our method for the drug incorporation into the micelles proceeded in two steps: solvent evaporation and sonication. We will denote micelles prepared by evaporation of TFE as "micelle A", and those prepared by evaporation of chloroform as "micelle B". Among them, samples containing different amounts of CPT were prepared, and they will be represented by how much wt.% CPT/polymer was used in the feed, i.e., 10% CPT, 20% CPT, and so on. Except for the solvent used in the film preparation, all other process factors were identical between micelles A and B. We varied the CPT/polymer ratio between 5 and 100% by weight, by adding an appropriate volume of 1 mg/mL CPT solution. Therefore, the total volume of the solvent was different for each sample, depending on the amount of CPT required.

3.2. Solubility of CPT in various solvents

We evaluated solubility of CPT in several organic solvents. We present the results with TFE, chloroform, and DMSO in Fig. 2 and omit other solvents for presentation clarity. In chloroform, the measured absorbance was similar to that in THF or DMSO up to 1 mg/mL, but it took a sudden jump at this concentration and went out of scale for [CPT] > 1 mg/mL. The solubility of CPT in THF and 1,4-dioxane was also poor as these solvents also gave high absorbance at 600 nm for even [CPT] < 1 mg/mL, and CPT was practically insoluble at the higher concentrations. On the other hand, CPT was well dissolved in TFE, DMSO, DMF, and DMAc. CPT was moderately soluble in 1,1,1-trifluoro-2-propanol and 1,1,1,3,3,3-hexafluoro isopropanol but not as soluble as TFE. From these results we concluded that

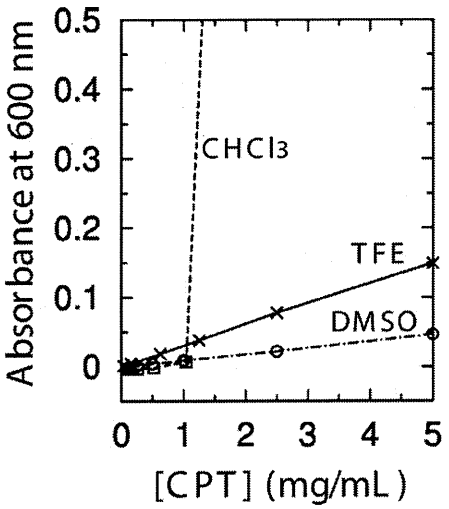

Fig. 2. Turbidity of CPT solutions in DMSO (○), TFE (×), and chloroform (□) as measured with a UV-VIS spectrometer.

the CPT solution used to prepare micelles should be in TFE or chloroform, and that [CPT] ≤1 mg/mL. One might consider the use of DMSO; however in our evaporation method, the solvent needs to be removed from the system. Therefore, solvents with a high boiling point are not preferred (b.p. DMSO = 189 °C, chloroform = 61 °C).

3.3. Characterization of CPT-incorporated micelles

3.3.1. Particle size determination by dynamic light scattering (DLS)

Fig. 3(a) shows the average Cumulant diameter of CPT micelles for various CPT amounts in the feed (5–100 wt.% with respect to polymers) as measured by DLS. The Cumulant average particle size ranged from ~80 to ~160 nm both for micelle A (prepared from TFE) and micelle B (prepared from CHCl3). The particle size of micelle B appeared to reach a limiting value of ~160 nm for a CPT/polymer weight ratio greater than 20%, whereas that of micelle A reached the first plateau between 20 and 40 wt.% CPT at ~110 nm, and then continued to increase to ~160 nm, reaching the second plateau between 40 and 60 wt.% CPT. Overall, the general tendency was that the particle size increased with the amount of CPT employed.

Fig. 4 shows the weight-weighted particle-size distribution of micelles prepared from 10 wt.% CPT/polymer as representative data. In Fig. 4(a), micelle A was observed to possess two peaks at 32 nm and 130 nm. Similarly, Fig. 4(b) corresponding to micelle B shows 2 peaks: one at 48 nm and the other at 168 nm, indicating that the aqueous micellar solutions contained two populations of particles. We assumed that the latter was a secondary association of micelles. In both of the micelle samples, the group of smaller particles constituted the majority (89% and 86% in weight for micelle A and micelle B, respectively) in the two populations.

3.3.2. CPT recovery in preparation of CPT-incorporated micelles

Fig. 3(b) shows CPT concentrations recovered in 4 mL of polymeric micelle aqueous solutions after the product was purified through centrifugation and filtration, plotted against the weight % of CPT/polymer in the feed. The same behaviors were observed between the average diameters shown in Fig. 3(a) and the CPT concentrations shown in Fig. 3(b) for both micelle A and micelle B. The CPT concentration in micelle B reached a plateau of ~20 wt.% CPT/polymer in the feed, where the maximum [CPT] value was ~80 μg/mL. This behavior was identical to the behavior of the Cumulant diameter shown in Fig. 3(a). Micelle A reached two

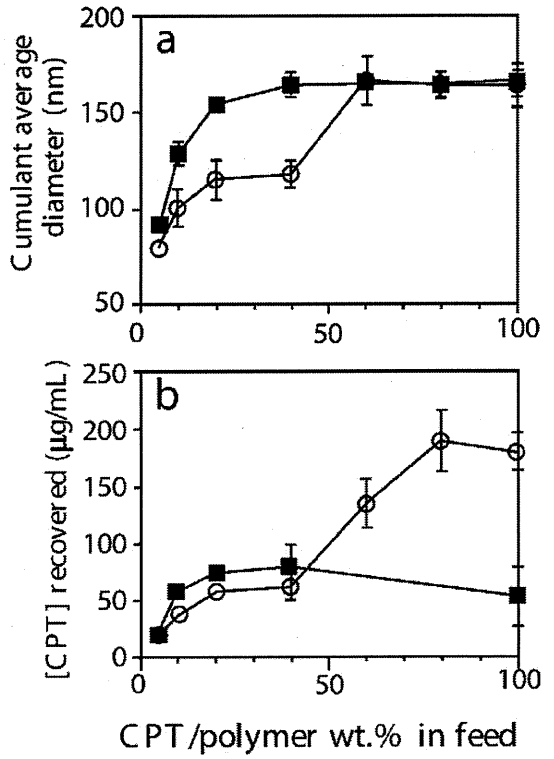

Fig. 3. CPT incorporation behaviors of polymeric micelles. (a) Cumulant average diameter of CPT micelles prepared with TFE(○, micelle A) or chloroform (■, micelle B). Data are shown in the average ± standard deviation of three measurements of the Cumulant average. (b) The CPT concentration recovered in an aqueous CPT micelle solution. Preparations of the micelles rested on TFE (○, micelle A) or chloroform (■, micelle B). Data are shown in the average ± standard deviation of three measurements.

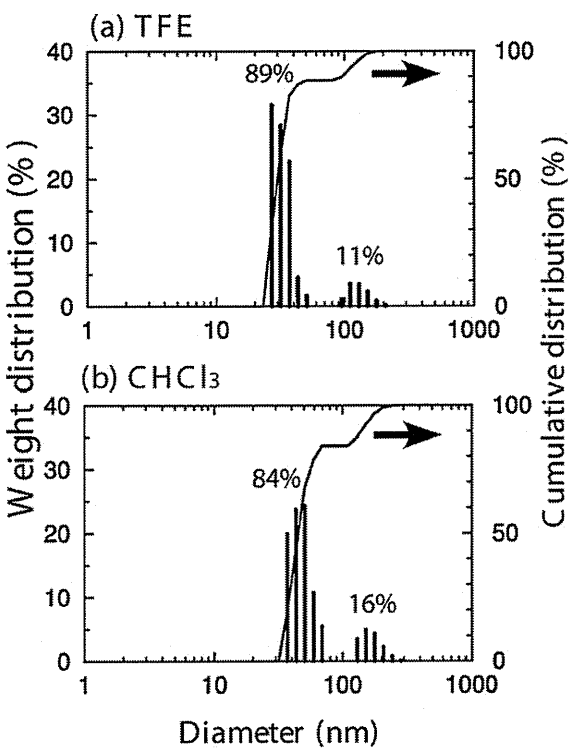

Fig. 4. Weight-weighted diameter distributions measured by dynamic light scattering for (a) micelle A (prepared from a solution in TFE) and (b) micelle B (prepared from a solution in chloroform). The CPT/polymer wt. ratio in the feed was 10% for the two cases. Values (%) shown in figures are weight proportions of the two peaks.

Table 1
CPT concentrations recovered after each step.

Solvent	CPT amounts in the feed[a]		[CPT] μg/mL after each step					
			Sonication→		Centrifugation→		Filtration	
TFE	0.5 mg	10 wt.%	120 ± 13	110	38 ± 5	31	5± 5	27
	2.0 mg	40 wt.%	470 ± 13	490	71 ±45	95	17 ±10	86
	5.0 mg	100 wt.%	I 1030 ±110	1100	66 ±10	170	27 ±12	160
CHCl3	0.5 mg	10 wt.%	89±23	140	8± 3	27	3± 0	27
	2.0 mg	40 wt.%	400 ± 44	560	18 ± 4	26	3± 1	25
	5.0 mg	100 wt.%	730 ± 24	1200	29 ±22	24	2± 1	23

Values at the left hand side are obtained without polymer and shown with the average ± S.D. ($n = 3$).Values at the right hand side are obtained with polymer ($n = 1$).
[a] CPT amounts are shown by weight for "without polymer" cases, and by CPT/polymer weight ratio in the feed for "with polymer" cases.

plateaus: the first one around 50 μg/mL at 20 wt.% CPT, and the second plateau around 190 μg/mL at 80 wt.% CPT. This was also the same behavior of the recovered CPT concentration shown in Fig. 3(a). In terms of efficiency (amount of CPT recovered/amount of CPT used), for micelle A, CPT was most efficiently recovered between levels of 5 and 10 wt.% CPT/polymer (~30% recovery), and efficiency of CPT recovery dropped to ~15% around 40 wt.% CPT, and then slightly improved in the 60–80 wt.% CPT range, and finally settled ~15% at 100 wt.% CPT/polymer. For micelle B, CPT recovery was highest at 10 wt.% CPT where ~45% of CPT used was recovered in the product, and then the efficiency of CPT recovery decreased steadily with the amount of CPT used. The lowest value in the range we examined in this study was only ~5% at 100 wt.% CPT. We treat the drop in the CPT recovery efficiency as a result of the precipitation of unincorporated CPT, as described below.

A series of experiments were conducted for estimation of the amount of unincorporated CPT. Concentrations of CPT in aqueous solutions were measured with a UV spectrometer after each step of the preparation procedure, namely, (1) the sonication step, (2) the centrifugation step, and (3) the filtration step. In these experiments, the procedure used for the CPT micelle preparation was carried out with and without the polymer. Table 1 summarizes results. The amount of CPT 0.5, 1.0, 2.0, or 5.0 mg in "without polymer" cases corresponded to 10, 20, 40, or 100% CPT/polymer ratios in "with polymer" cases. After the sonication step, considerably high amounts of CPT (ca. 60–100%) were recovered in both "with polymer" and "without polymer" cases, as revealed by the large values in Table 1's sonication columns. For "without polymer" cases, most of the recovered CPT seemed to be present as dispersion of small insoluble aggregates because the obtained solutions were turbid. Therefore, after the centrifugation step, the recovered CPT concentrations substantially dropped to 8–29 μg/mL for CHCl3 solvent cases and 38–71 μg/mL for TFE solvent cases owing to precipitation of the insoluble aggregates. In contrast, for "with polymer" cases, the recovered CPT amounts exhibited little change through the filtration step, while a considerable drop was observed in the "without polymer" cases after the filtration step possibly because of adsorption of the insoluble aggregates on a filter membrane

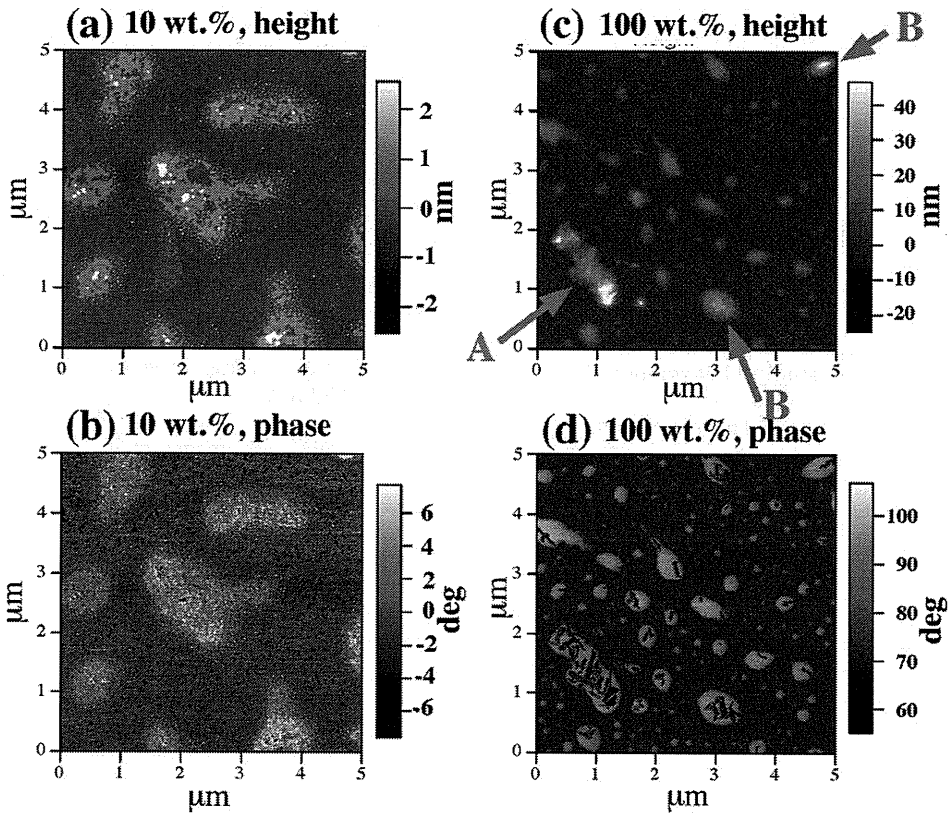

Fig. 5. AFM images of micelle A (prepared from a solution in TFE). The CPT/polymer wt.% in the feed was either 10% (a and b) or 100% (c and d). Images (a) and (c) are of height, while (b) and (d) concern phases.

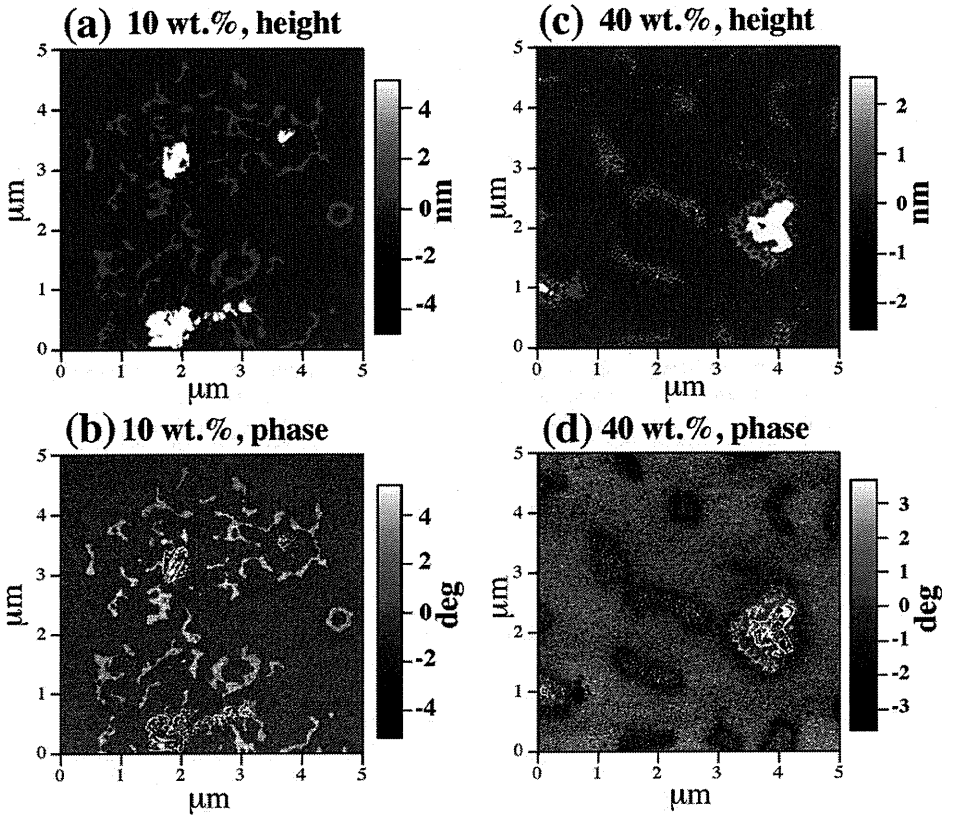

Fig. 6. AFM images of micelle B (prepared from a solution in chloroform). The CPT/polymer wt.% in the feed was either 10% (a and b) or 40% (c and d). Images (a) and (c) are of height, while (b) and (d) concern phases.

through hydrophobic interactions. These results indicate that most of the recovered CPT in the micelle solutions was incorporated into the polymeric micelles, and that low efficiency of the CPT incorporation at high CPT-polymer ratios resulted from the presence of large amounts of unincorporated CPT.

3.3.3. *Morphological observation of CPT-incorporated polymeric micelles by AFM*

AFM images of micelles are shown in Figs. 5 and 6. We obtained images by using dried films: aqueous micelle solutions were deposited on mica, and then the mica surfaces were rinsed with Millipore water for removal of excess sample, and finally dry nitrogen gas served to dry the surfaces. These dried films may not represent the real status of micelles in solution, but still provide useful topographical information on the samples.

A 5 μm × 5 μm scan of a film prepared from micelle A (10 wt.% CPT/polymer) shows patches of high contrast areas (Fig. 5, both height (a) and phase (b) images). The patches varied in size, but most of them occupied several hundred nm by several hundred nm to a few microns of area. The patches were relatively flat areas surrounded by small round-shaped islands less than 30 nm in diameter. Some islands were found also within patches; these spots were ~5–20 nm tall with respect to the surrounding flat area, whereas the flat area was <5 nm high with respect to the lowest part of the sample. In these images, we could not assign polymer locations or CPT locations.

Interesting images were observed in a film of micelle A prepared from a 100 wt.% CPT/polymer ratio (Fig. 5(c) and (d)). In the height image (Fig. 5(c)), round objects of various sizes ranging from ~10 nm to several hundred nm in diameter were present, along with larger elliptical objects. The cross-section of this image showed that the height difference between the dark area and the top of the largest island (pointed at with arrow A) was approximately 30 nm. In some other areas, smaller objects with brighter contrast were observed (pointed at with arrow B), indicating the existence of a different species from that of the round area. In the corresponding phase image (Fig. 5(d)), round objects in bright contrast were found at the same positions and in the same sizes as those in the height image, and in addition to these islands were observed rectangular objects of dark contrast on top of those islands. Judging from this image's phase intensity (gray scale bar on the side), the hardness of the rectangular areas was similar to that of the background (most likely bare mica, possible with some polymer coating), while the bright area was softer than the dark areas. We believe that the bright areas represent the polymer, and the dark rectangular areas represent the crystals of CPT. These crystal-like rods were ~0.1 μm × 1 μm or smaller, and were positioned on top of the polymer islands.

Fig. 6 shows AFM images of micelle B prepared from either 10 wt.% (a,b) CPT/polymer or 40 wt.% (c,d) CPT/polymer in the feed. Fig. 6(a) represents a height image obtained from micelle B prepared at a 10 wt.% CPT/polymer ratio. In this 5 μm × 5 μm image, the sample appears to have two distinct areas: string-like structures that are <5 nm tall with respect to the lowest point of the substrate, and areas of much higher contrast, ~50 nm tall with respect to the surrounding area. In the phase image, the latter structure seems to be a collection of smaller lumps whose contrast differs from the string-like structures. When the height contrast was optimized for these tall lumps (image not shown here), the rectangular rods were the same shape as that of the crystal-like structure in Fig. 5(d). Although these AFM measurements with the dried films may cause artifacts in the film preparation process, these results suggest two matters. One, CPT molecules formed crystals in a high CPR/polymer feed ratio. Second, empty (incorporating no

CPT molecules) polymeric micelles may be present more probably in a high CPR/polymer feed ratio.

Fig. 6(c) and (d) were obtained from micelle B prepared in CPT/polymer 40 wt.%. These images were similar to Fig. 5(a) and (b) obtained from micelle A prepared from 10 wt.% CPT/polymer in TFE. The patches that were <5 nm in height with respect to the lowest part of the substrate were ubiquitous and were similar to those of micelle A; however, in addition to these patches, rod-like structures of ~10–40 nm thickness compared to the surroundings were found. These rod-like objects were the same as those seen in Fig. 6(a) and (b). These results suggest that aggregation of CPT molecules occurred in micelle B in a more drastic manner than micelle A, and that the empty micelles were present in micelle B in a higher proportion than micelle A.

3.3.4. CPT in micelle solutions monitored by UV–vis spectroscopy

As described earlier, the amount of CPT contained in a micelle solution was determined in a mixture of DMSO and water (9:1, vol./vol.) by UV–vis spectroscopy. This mixed solvent dissolves both CPT and the hydrophobic block of the copolymer. Therefore, CPT molecules that were released from the polymeric micelles were measured in this mixed solvent. For such a measurement only the peak intensity was necessary, but we now turn to the spectrum itself measured in water to examine the environment that surrounds CPT. Fig. 7 shows UV spectra of aqueous CPT-incorporated micelle solutions prepared at various CPT/polymer ratios by the use of (a) TFE and (b) chloroform as a solvent in the micelle preparation. CPT micelle solutions were diluted to a 1/10 concentration in water, corresponding to a CPT concentration of ~2–20 μg/mL and corresponding to a polymer concentration of ~0.1 mg/mL that was much higher than polymer's critical micelle concentration (Yamamoto et al., 2007). The spectra were normalized at a peak intensity of 351.5 nm. There were two main peaks in the spectra, as shown in Fig. 7: 351.5 nm and 367.5 nm. The shoulder peak around 395 nm, which was prominent in 60–100 wt.% CPT/polymer in micelle A, suggests intermolecular association of CPT molecules. The same shoulder was also observed in micelle B for a CPT/polymer wt.% range of 20–100%, but to a lesser degree than micelle A. The hypochromic effect was also observed at 367.5 nm, where the peak intensity decreased for some of the samples, compared with that of 5% CPT/polymer samples. This also indicates the intermolecular association of CPTs' aromatic chromophores.

3.3.5. Polarization degree of CPT molecules in the polymeric micelles

We evaluated the polarization degree of CPT molecules in the polymeric micelles by measuring the fluorescence anisotropy value (r). Fig. 8 shows the fluorescence anisotropy of CPT molecules in various CPT concentrations. The polarization degree reflects environments of incorporated CPT molecules. For polymeric micelle samples PEG-P(Asp(Bzl 70)) and PEG-P(Asp(Bzl 82)), the concentration of polymer was constant at 1.67 mg/mL, while CPT concentrations were varied through adjustments of CPT quantity used in the incorporation procedure into the micelles. Two influencing factors are present for the polarization degree; mobility/rigidity of environments where fluorescence molecules are present, and fluorescence extinction by the other fluorescence molecules. A greater polarization degree is observed for the fluorescence molecules in the more rigid (=less mobile) environments, while the polarization degree can change (raised or lowered) through the extinction by the other fluorescence molecules. Usually, the mobility/rigidity is the determining factor for the polarization degree of molecules incorporated in polymeric micelle inner cores, since it is obvious that the CPT molecules incorporated into the micelle inner core exist in a more rigid environment than the one where free CPT molecules dissolved in DMSO. (DMSO

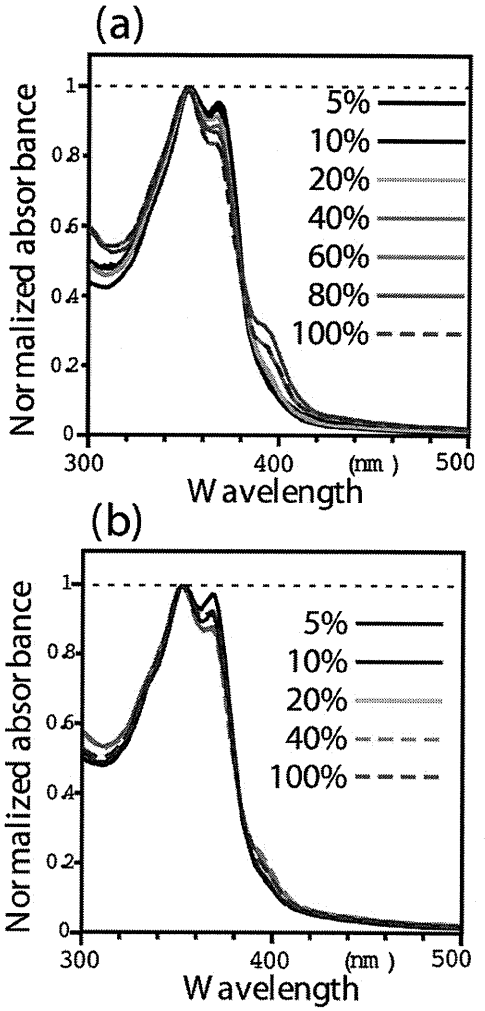

Fig. 7. Normalized UV spectra of CPT-incorporated micelles in aqueous solutions: (a) micelle A (prepared from a solution in TFE), and (b) micelle B (prepared from a solution in chloroform). The percentages shown in figures indicate the CPT/polymer wt.% in the feed.

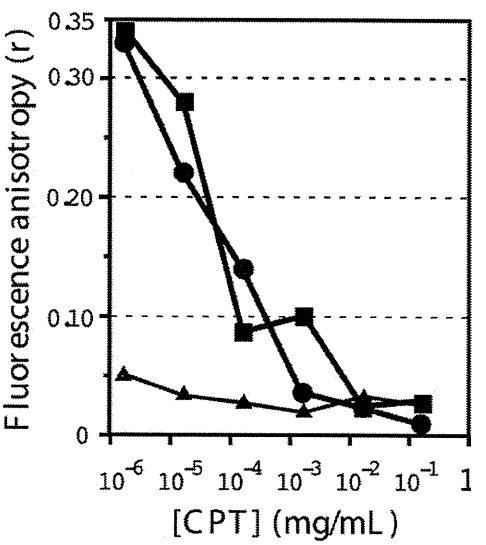

Fig. 8. Polarization degree of CPT fluorescence. CPT in polymeric micelles forming from PEG-P(Asp(Bzl 70): ●, in polymeric micelles forming from PEG-P(Asp(Bzl 82): ■, and CPT just dissolved in DMSO: ▲.

is a good solvent as proven in Fig. 2.) Unexpectedly, for these two polymeric micelle samples, the CPT polarization degrees were almost the same as or lower than the polarization degrees of free (unincorporated) CPT molecules dissolved in DMSO at high CPT concentrations of 1.7×10^{-1} and 1.7×10^{-2} mg/mL. This indicates that the fluorescence extinction was the determining factor in this CPT concentration range in a different manner from the usual polymeric micelle cases where the mobility/rigidity is the determining factor. In fact, the polarization degrees of the polymeric micelle samples were observed to become greater as the CPT concentration was lowered, while the polarization degrees were almost constant for the free CPT solution in DMSO in the whole measurement range. This tells two matters. One, the rigid micelle inner core environment was confirmed, as already reported with a dipyrene fluorescence probe (Yamamoto et al., 2007). Second, the polarization of CPT molecules can be detected, but only in much lower CPT concentration ranges than those used in actual formulations for in vitro and in vivo evaluations where a high CPT content (ca. 1–40 CPT wt. %) is preferably applied. Irrespective of this gap in the CPT concentration range, these results are the first information concerning drug molecule's incorporation status in the polymeric micelle inner core. By referring to this fact, we carried out the following polarized fluorescence microscopy measurements in this low CPT concentration range as described in the next section.

3.3.6. *Polarized fluorescence microscopy*

In order to detect the polarized fluorescence of CPT molecules, we carried out polarized fluorescence microscopy measurements on a quartz plate with a dried micelle sample having a low CPT/polymer ratio (0.001%, which corresponds to the micelle prepared at 1.7×10^{-5} mg/kg [CPT] in Fig. 8). At the emission side, the perpendicularly polarized component of the fluorescence signal was selectively observed with a supersensitive CCD camera, while at the excitation side an Ar-ion laser was applied with a polarization controller. As shown in Fig. 9, two bright spots were observed in this area, and fluorescence intensities of these two spots were found to change in accordance with the polarization controller angle. For spots A and B, both the brightest and darkest signals appeared with exactly 180° intervals. Therefore, it was revealed that this measurement detected the polarized fluorescence of the CPT molecules. This is the first direct visualization of the polarity of the drug molecules incorporated in polymeric micelles. Bright spots were not observed at higher CPT/polymer ratios (0.1%, 1%, and 10%, data not shown) owing to the florescence extinction observed in the polarized fluorescence spectra shown in Fig. 8. Therefore, this method could not reveal morphologies of the CPT molecules at the high CPT/polymer ratios that were used for in vitro and in vivo evaluations. The fluorescence extinction behaviors are dependent on excitation/emission characteristics of molecules; therefore, this method may be applied to drug molecules exhibiting prominent extinction behaviors. This polarized fluorescence technique can be a powerful and direct method to analyze morphologies of drug molecules in the micelle inner core.

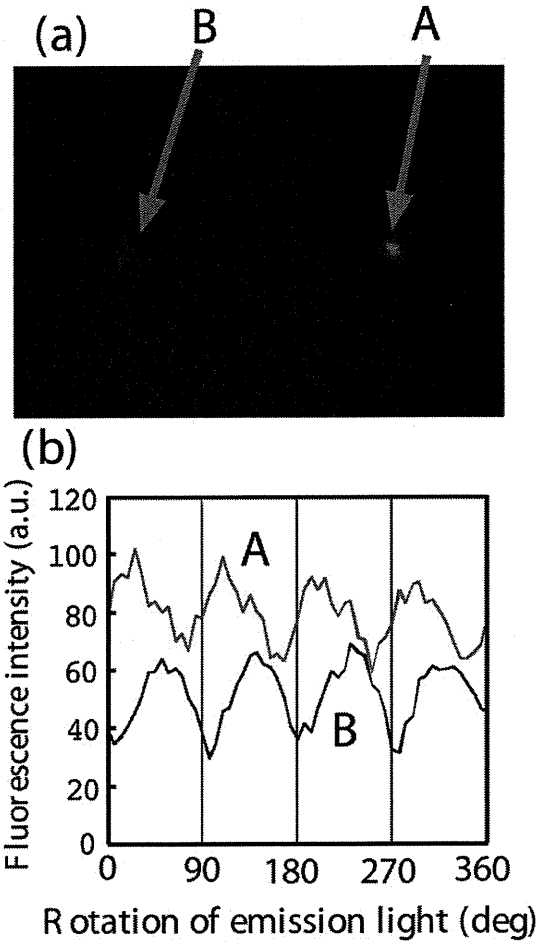

Fig. 9. Polarization fluorescence microscopic image (a) and its intensity change relative to the rotation of polarized emission light (b).

3.4. *Determination of CPT concentrations in plasma*

In Table 2, we summarize results of CPT concentrations in plasma at 4 h after intravenous injection of the CPT-incorporated polymeric micelles. We previously examined time course profiles in blood of [CPT] in polymeric micelles, and reported that CPT micelles prepared from PEG-P(Asp(Bzl 75)) exhibited the best in vivo stability value (9.3% dose) among similar polymers of various percentages of benzyl groups attached at the hydroxyl groups of P(Asp) (Watanabe et al., 2006). In this Table, we compare the values obtained from this previous report with our new results. In the previous method, CPT was incorporated by the use of chloroform as the evaporation solvent. We also observed that the CPT/polymer ratio did not affect so much (7.6 and 5.3% doses) the CPT concentrations in blood when we were using PEG-P(Asp(Bzl 57)), and

Table 2
CPT concentrations in blood 4 h after intravenous injection of polymeric micelles.

polymer	CPT/polymer wt. ratio in feed	solvent used for incorporation	CPT in blood (% dose)	reference
PEG-P(Asp(Bzl 74))	10%	TFE	27.3 ± 2.6	
PEG-P(Asp(Bzl 74))	5%	TFE	28.6 ± 0.5	
PEG-P(Asp(Bzl 75))	40%	Chloroform	9.3 ± 1.8	Watanabe et al., 2006
PEG-P(Asp(Bzl 57))	40%	Chloroform	7.6 ± 0.8	
PEG-P(Asp(Bzl 57))	10%	Chloroform	5.3 ± 0.6	

Table 3
Cohesion parameters of CPT, solvents, and an inner-core-forming polymer block.

	δD	δP	δH	δt
CPT	25.8	6.8	8.9	28.1
TFE	15.4	8.3	16.4	24.0
chloroform	17.8	3.1	5.7	18.9
DMSO	18.4	16.4	10.2	26.7
P(Asp) block	23.2	22.2	13.4	34.8
P(Asp (Bzl 74)) block	24.9	10.4	8.1	28.2

δD: dispersion solubility parameter.δP: Polar solubility parameter.δH: hydrogen bonding solubility parameter.δt: total (hildebrand) solubility parameter; $\delta t = (\delta D^2 + \delta P^2 + \delta H^2)^{1/2}$.Parameters are calculated according to methods and values of a reference (Hansen, 2007 Parameters of TFE, chloroform, and DMSO were taken from the reference. The units are: $(J\,cm^{-3})^{1/2}$.

that the CPT concentration did not exceed a 10% dose for the CPT-incorporated micelles prepared with chloroform. In contrast, with the polymeric micelles prepared from TFE, we obtained significantly higher CPT concentrations around the 28% dose. When we varied the CPT/polymer levels between 5% and 10%, no change in the CPT concentrations was observed. All these results indicate that the choice of organic solvent is an important key to obtaining the stable circulation of incorporated drugs in blood.

4. Discussion

In polymeric micelle research for drug delivery systems, most efforts have been made in carrier polymer design and preferable choice of the carrier polymer-drug combinations for the targetable carrier systems. The drug-incorporation process may be a very important step in preparing various polymeric micelle drug carrier systems; however, examinations of the topic are scarce. In this paper, we reported that the solvent used for the drug-incorporation process into polymeric micelles had substantial effects on drug-incorporation efficiency, micelle diameter, morphologies of the micelles and of the incorporated drug, and in vivo pharmacokinetic behavior of the incorporated drug. In particular, considerable prolongation of circulation in the bloodstream, which is essential for passive tumor targeting, was successfully obtained by the choice of an appropriate organic solvent used in the evaporation-"drug incorporation" method. As far as we know, this is the first indication of the solvent's importance for the prolongation of circulation in blood of polymeric micelle targeting systems.

When we used 2,2,2-trifluoroethanol (TFE) for the incorporation solvent, we obtained smaller average diameters of the micelles (in a drug/polymer ratio range from 5 wt.% to 40 wt.%) and more stable circulation in blood than the micelles did when prepared by the use of chloroform as the incorporation solvent. We think that the higher CPT solubility of TFE at CPT concentrations higher than 1 mg/mL is the reason for the preferable micelle formulation that exhibited the more stable circulation in blood than that of the chloroform case. Here, we conducted solubility and miscibility estimations by calculating solubility parameters. Table 3 lists the cohesion parameters of the materials: CPT, the solvents used in our experiment, and the hydrophobic block of the polymer. Theoretically, the smaller the difference between the δt of the drug and the solvent, the more soluble the drug is in the solvent (Huynh et al., 2008). If that is the case, the solubility of the three solvents' CPT is, from greater to smaller, DMSO > TFE > chloroform. This is in agreement with the results obtained from the turbidity experiment. Furthermore, the cohesion parameters of CPT are quite similar to those of the P(Asp(Bzl 74)) block of the polymer. This block copolymer PEG-P(Asp(Bzl 74) has been chosen from among several compositions and other hydrophobic moiety structures in terms of stable drug incorporation of CPT (Yokoyama et al., 2004; Yamamoto et al., 2007). Therefore, the calculated value agrees well with this fact. It is expected that the drug incorporation into the micelle inner core is of higher efficiency and is more stable when the drug is more miscible with the inner core-forming hydrophobic polymer block. However, more examinations with various combinations of the drug and the inner core-forming block are required for valuable applications of solubility-parameter calculations to reliable estimations of the optimized combination of a given drug and with a given carrier polymer.

We consider that the TFE's higher solubility of CPT efficiently inhibits large aggregates' formation of CPT molecules, resulting in higher CPT-incorporation yields and in the smaller micelle diameters than is the case with chloroform. AFM images in Fig. 6 indicate the presence of many empty micelles that do not contain CPT. This can be because large CPT aggregates formed aggressively during the solvent evaporation of chloroform, resulting in a large amount of unincorporated CPT aggregates.

As discussed above, this paper presents a novel methodology in polymeric micelle carrier systems for better formulations regarding the choice of an appropriate solvent in the evaporation drug-incorporation process. This is a very simple approach, but is no less important for being simple because the choice considerably changed pharmacokinetic behavior, as demonstrated in Table 3.

In addition to the importance of the solvent choice, this paper provided the first morphological information on incorporated drugs in polymeric micelles' inner cores. In general, morphological analyses of incorporated drugs are very difficult owing to the very small size of micelle inner cores (several nm). In this paper, we have shown the presence of the polarized CPT molecules in the inner cores by measuring fluorescence polarization spectra and microscopic images, as well as by measuring the formation of CPT crystals through AFM observations. We believe these morphological factors are very important for optimized drug incorporation into the polymeric micelle carriers although technical difficulties prevented us from identifying direct morphological evidence for stable CPT incorporation in the TFE case.

5. Conclusion

We observed substantial effects that solvents used in drug-incorporation processes can have on drug-incorporation behaviors, on the morphologies of both the incorporated drug and the polymeric micelles, and on pharmacokinetic behaviors. Simply through an appropriate choice of solvent, the circulation of an incorporated drug in blood was greatly improved for tumor targeting. Morphological analyses of the inner core revealed the directed alignment of the CPT molecules and CPT crystals in the micelle inner core at a low and high CPT/polymer ratio, respectively. These analyses are important for further developments of polymeric micelle drug-carrier systems.

Acknowledgements

This work was supported by the Ministry of Health, Labor, and Welfare of Japan and by both the JST CREST program and Grant-in-Aid of the Ministry of Education, Culture, Sports, Science, and Technology of Japan. Y. Harada, T. Yamamoto, and M. Yokoyama acknowledge the support from the Program for Promoting the Establishment of Strategic Research Centers, Special Coordination Funds for Promoting Science and Technology, and the Ministry of Education, Culture, Sports, Science and Technology of Japan. We thank Asylum Technology Co., LTD., Tokyo, Japan for providing access to an Atomic Force Microscopy MFP-3D.

References

Aliabadi, H.M., Lavasanifar, A., 2006. Polymeric micelles for drug delivery. Expert Opin. Drug Deliv. 3, 139–162.

Bader, H., Ringsdorf, H., Schmidt, B., 1984. Watersoluble polymers in medicine. Angew. Chem. 123/124, 457–485.

Chansri, N., Kawakami, S., Yokoyama, M., Yamamoto, T., Charoensit, P., Hashida, M., 2008. Anti-tumor effect of all-*trans* retinoic acid loaded polymeric micelles in solid tumor bearing mice. Pharm. Res. 25, 428–434.

Forrest, M.L., Won, C.Y., Malick, A.W., Kwon, G.S., 2006a. In vitro release of the mTOR inhibitor rapamycin from poly(ethylene glycol)-*b*-poly(ε-caprolactone) micelles. J. Contr. Rel. 110, 370–377.

Forrest, M.L., Zhao, A., Won, C.Y., Malick, A.W., Kwon, G.S., 2006b. Lipophilic prodrugs of Hsp90 inhibitor geldanamycin for nanoencapsulation in poly(ethylene glycol)-*b*-poly(ε-caprolactone) micelles. J. Contr. Rel. 116, 139–149.

Hamaguchi, T., Matsumura, Y., Suzuki, M., Shimizu, K., Goda, R., Nakamura, I., Nakatomi, I., Yokoyama, M., Kataoka, K., Kakizoe, T., NK105, 2005. A paclitaxel-incorporating micellar nanoparticle formulation, can extend in vivo antitumour activity and reduce the neurotoxicity of paclitaxel. Br. J. Cancer 92, 1240–1246.

Hamaguchi, T., Kato, K., Yasui, H., Morizane, C., Ikeda, M., Ueno, H., Muro, K., Yamada, Y., Okusaka, T., Shirao, K., Shimada, Y., Nakahama, H., Matsumura, Y., 2007. A phase I and pharmacokinetic study of NK105, a paclitaxel-incorporating micellar nanoparticle formulation. Br. J. Cancer 97, 170–176.

Huynh, L., Grant, J., Leroux, J.-P., Delmas, P., Allen, C., 2008. Predicting the solubility of the anti-cancer agent docetaxel in small molecule excipients using computational methods. Pharm. Res. 25, 147–157.

Kawano, K., Watanabe, M., Yamamoto, T., Yokoyama, M., Opanasopit, P., Okano, T., Maitani, Y., 2006. Enhanced antitumor effect of camptothecin loaded in long-circulating polymeric micelles. J. Contr. Rel. 112, 329–332.

Hansen, C.M., 2007. Hansen Solubility Parameters; A User's Handbook, second ed. CRC Press, Boca Raton.

Koizumi, F., Kitagawa, M., Negishi, T., Onda, T., Matsumoto, S., Hamaguchi, T., Matsumura, Y., 2006. Novel SN-38-incorporating polymeric micelles, NK012, eradicate vascular endothelial growth factor-secreting bulky tumors. Cancer Res. 66, 10048–10056.

Kwon, G.S., Naito, M., Kataoka, K., Yokoyama, M., Sakurai, Y., Okano, T., 1994a. Block copolymer micelles as vehicles for hydrophobic drugs. Colloids Surf. B: Biointerf. 2, 429–434.

Kwon, G.S., Suwa, S., Yokoyama, M., Okano, T., Sakurai, Y., Kataoka, K., 1994b. Enhanced tumor accumulation and prolonged circulation times of micelle-forming poly(ethylene oxide–aspartate) block copolymer–adriamycin conjugates. J. Contr. Rel. 29, 17–23.

Maeda, H., Seymour, L.W., Miyamoto, Y., 1992. Conjugates of anticancer agents and polymers: Advantages of macromolecular therapeutics in vivo. Bioconjugate Chem. 3, 351–361.

Matsumura, Y., Maeda, H., 1986. A new concept for macromolecular therapeutics in cancer chemotherapy: Mechanism of tumoritropic accumulation of proteins and the antitumor agent smancs. Cancer Res. 46, 6387–6392.

Matsumura, Y., Hamaguchi, T., Ura, T., Muro, K., Yamada, Y., Shimada, Y., Shirao, K., Okusaka, T., Ueno, H., Ikeda, M., Watanabe, N., 2004. Phase I clinical trial and pharmacokinetic evaluation of NK911, a micelle-encapsulated doxorubicin. Br. J. Cancer 91, 1775–1781.

Molavi, O., Ma, Z., Mahmud, A., Alshamsan, A., Samuel, J., Lai, R., Kwon, G.S., Lavasanifar, A., 2008. Polymeric micelles for the solubilization and delivery of STAT3 inhibitor cucurbitacins in solid tumors. Int. J. Pharm. 347, 118–127.

Nakajima, T.E., Yanagihara, K., Takigahira, M., Yasunaga, M., Kato, K., Hamaguchi, T., Yamada, Y., Shimada, Y., Mihara, K., Ochiya, T., Matsumura, Y., 2008a. Antitumor effect of SN-38-releasing polymeric micelles, NK012, on spontaneous peritoneal metastases from orthotopic gastric cancer in mice compared with irinotecan. Cancer Res. 68, 9318–9322.

Nakajima, T.E., Yasunaga, M., Kano, Y., Koizumi, F., Kato, K., Hamaguchi, T., Yamada, Y., Shirao, K., Shimada, Y., Matsumura, Y., 2008b. Synergistic antitumor activity of the novel SN-38-incorporating polymeric micelles, NK012, combined with 5-fluorouracil in a mouse model of colorectal cancer, as compared with that of irinotecan plus 5-fluorouracil. Int. J. Cancer 122, 2148–2153.

Nishiyama, N., Okazaki, S., Cabral, H., Miyamoto, M., Kato, Y., Sugiyama, Y., Nishio, K., Matsumura, Y., Kataoka, K., 2003. Novel cisplatin-incorporated polymeric micelles can eradicate solid tumors in mice. Cancer Res. 63, 8977–8983.

Okuda, T., Kawakami, S., Yokoyama, M., Yamamoto, T., Yamashita, F., Hashida, M., 2008. Block copolymer design for stable encapsulation of N-(4-hydroxyphenyl)retinamide into polymeric micelles in mice. Int. J. Pharm. 357, 318–322.

Okuda, T., Kawakami, S., Higuchi, Y., Satoh, T., Oka, Y., Yokoyama, M., Yamashita, F., Hashida, M., 2009. Enhanced in vivo antitumor efficacy of fenretinide encapsulated in polymeric micelles. Int. J. Pharm. 373, 100–106.

Opanasopit, P., Yokoyama, M., Watanabe, M., Kawano, K., Maitani, Y., Okano, T., 2004. Block copolymer design for camptothecin incorporation into polymeric micelles for passive tumor targeting. Pharm. Res. 21, 2003–2010.

Shin, H.C., Alani, A.W., Rao, D.A., Rockich, N.C., Kwon, G.S., 2009. Multi-drug loaded polymeric micelles for simultaneous delivery of poorly soluble anticancer drugs. J. Contr. Rel. 140, 294–300.

Tuzar, Z., Kratochvil, P., 1976. Block and graft copolymer micelles in solution. Adv. Colloid Interf. Sci. 6, 201–232.

Yamamoto, Y., Yokoyama, M., Opanasopit, P., Hayama, A., Kawano, K., Maitani, Y., 2007. What are determining factors for stable drug incorporation into polymeric micelle carriers? Consideration on physical and chemical characters of the micelle inner core. J. Contr. Rel. 123, 11–18.

Yokoyama, M., Inoue, S., Kataoka, K., Yui, N., Okano, T., Sakurai, Y., 1989. Molecular design for missile drug: Synthesis of adriamycin conjugated with IgG using poly(ethylene glycol)-poly(aspartic acid) block copolymer as intermediate carrier. Die Makromolekulare Chemie 190, 2041–2054.

Yokoyama, M., Okano, T., Sakurai, Y., Ekimoto, H., Shibazaki, C., Kataoka, K., 1991. Toxicity and antitumor activity against solid tumors of micelle-forming polymeric anticancer drug and its extremely long circulation in blood. Cancer Res. 51, 3229–3236.

Yokoyama, M., Okano, T., Sakurai, Y., Kataoka, K., 1994. Improved synthesis of adriamycin-conjugated poly(ethylene oxide)-poly(aspartic acid) block copolymer and formation of unimodal micellar structure with controlled amount of physically entrapped adriamycin. J. Contr. Rel. 32, 269–277.

Yokoyama, M., Okano, T., Sakurai, Y., Fukushima, S., Okamoto, K., Kataoka, K., 1999. Selective delivery of adriamycin to a solid tumor using a polymeric micelle carrier system. J. Drug Targeting 7, 171–186.

Yokoyama, M., Opanasopit, P., Maitani, Y., Kawano, K., Okano, T., 2004. Polymer design and incorporation method for polymeric micelle carrier system containing water-insoluble anti-cancer agent camptothecin. J. Drug Targeting 12, 373–384.

Yokoyama, M., 2005. Polymeric Micelles for the Targeting of Hydrophobic Drugs. In: Kwon, G.S. (Ed.), Drug and Pharmaceutical Sciences, Vol. 148, Polymeric Drug Delivery Systems. Taylor & Francis, Boca Raton, pp. 533–575.

Yokoyama, M., 2007. Polymeric micelles as nano-sized drug carrier systems. In: Domb, A.J., Tabata, Y., Kumar, M.N.V.R., Farber, S. (Eds.), Nanoparticles for Pharmaceutical Applications. American Scientific Publishers, Stevenson Ranch, pp. 63–72.

Watanabe, M., Kawano, K., Yokoyama, M., Opanasopit, P., Okano, T., Maitani, Y., 2006. Preparation of camptothecin-loaded polymeric micelles and evaluation of their incorporation and circulation stability. Int. J. Pharm. 308, 183–189.

International Journal of Pharmaceutics 421 (2011) 379–387

Contents lists available at SciVerse ScienceDirect

International Journal of Pharmaceutics

journal homepage: www.elsevier.com/locate/ijpharm

A facile preparation method of a PFC-containing nano-sized emulsion for theranostics of solid tumors

Kouichi Shiraishi[a], Reiko Endoh[a], Hiroshi Furuhata[a], Masamichi Nishihara[b], Ryo Suzuki[c], Kazuo Maruyama[c], Yusuke Oda[c], Jun-ichiro Jo[d], Yasuhiko Tabata[d], Jun Yamamoto[e], Masayuki Yokoyama[a,*]

[a] Medical Engineering Laboratory, Research Center for Medical Science, The Jikei University School of Medicine, 3-25-8, Nishi-shinbashi, Minato-ku, Tokyo 105-8461, Japan
[b] International Institute for Carbon-Neutral Energy Research (I²CNER), Kyushu University, 744 Motooka, Nishi-ku, Fukuoka 819-0395, Japan
[c] Department of Biopharmaceutics, School of Pharmaceutical Sciences, Teikyo University, 1091-1 Suwarashi, Midori-ku, Sagamihara, Kanagawa 252-5195, Japan
[d] Department of Biomaterials, Institute for Frontier Medical Sciences, Kyoto University, 53 Kawara-cho Shogoin, Sakyo-ku, Kyoto 606-8507, Japan
[e] Division of Physics and Astronomy, Graduate School of Science, Kyoto University, Kitashirakawa Oiwake-cho, Sakyo-ku, Kyoto 606-8502, Japan

ARTICLE INFO

Article history:
Received 14 June 2011
Received in revised form 27 August 2011
Accepted 2 October 2011
Available online 15 October 2011

Keywords:
Theranostics
Tumor targeting
Ultrasound
Perfluorocarbon
Emulsion

ABSTRACT

Theranostics means a therapy conducted in a diagnosis-guided manner. For theranostics of solid tumors by means of ultrasound, we designed a nano-sized emulsion containing perfluoropentane (PFC5). This emulsion can be delivered into tumor tissues through the tumor vasculatures owing to its nano-size, and the emulsion is transformed into a micron-sized bubble upon sonication through phase transition of PFC5. The micron-sized bubbles can more efficiently absorb ultrasonic energy for better diagnostic images and can exhibit more efficient ultrasound-driven therapeutic effects than nano-sized bubbles. For more efficient tumor delivery, smaller size is preferable, yet the preparation of a smaller emulsion is technically more difficult. In this paper, we used a bath-type sonicator to successfully obtain small PFC5-containing emulsions in a diameter of ca. 200 nm. Additionally, we prepared these small emulsions at 40 °C, which is above the boiling temperature of PFC5. Accordingly, we succeeded in obtaining very small nano-emulsions for theranostics through a very facile method.

1. Introduction

'Theranostics', 'theranosis', or 'theragnosis' is a newly created term in the fields of imaging diagnosis and drug delivery systems. As a word, 'theranostics' (Chen, 2011; Lammers et al., 2010, 2011; MacKay and Li, 2010) is a combination of therapy and diagnosis, and is defined as therapy conducted in a diagnosis-guided manner. A typical example of theranostics is found in a carrier system containing both a contrast agent for diagnosis and a drug for therapy. Theranostics has been studied with various types of drug carriers including liposomes (Kamaly and Miller, 2010), small molecules (Kalber et al., 2011), nano-particles (Jeong et al., 2011; Kim et al., 2010), emulsions (Gianella et al., 2011), synthetic polymers (Bryson et al., 2009), polymeric micelles (Blanco et al., 2009; Kaida et al., 2010; Min et al., 2010; Nakamura et al., 2006; Shiraishi et al., 2009, 2010), and other nano-sized carrier systems (Ai, 2011; Moon et al., 2011; Pan et al., 2008; Sanson et al., 2011). Ultrasound is considered to be a preferable modality for theranostics because ultrasound has been well studied and developed for image diagnoses and local therapies such as ultrasound lithotresis and hyperthermia.

For theranostics of solid tumors, micron-sized bubbles (microbubbles) (Hernot and Klibanov, 2008; Schutt et al., 2003; Unger et al., 2004) have been actively studied because the bubbles provide strong contrasts in ultrasonic images, and because cavitation of microbubbles (Grishenkov et al., 2009) induced by ultrasound can effectively damage cells. Cells can be damaged by both jet-stream and heat that are generated in the bubbles' cavitation. In the design of microbubbles for tumor applications, the size of the microbubbles is a very important factor. Larger microbubbles can produce stronger ultrasound image contrasts. In contrast, smaller bubbles are preferred for efficient delivery into tumor tissues because the size of the trans-vascular passage from the bloodstream into the tumor interstitial space is of a diameter smaller than 1 μm. It is believed that the maximum diameter for efficient translocation into tumor tissues is 200–400 nm (Ishida et al., 1999; Litzinger et al., 1994; Nagayasu et al., 1996; Yuan et al., 1995). (In this diameter range, bubbles must be called nano-bubbles.) This is an essential dilemma concerning the size of bubbles used for

Abbreviations: PFC, perfluorocarbon; PFC5, perfluoropentane; PFC6, perfluorohexane; DBU, 1,8-diazabicyclo[5.4.0]undec-7-ene; PEG-P(Asp(C7F9)x), poly(ethylene glycol)-b-poly(4,4,5,5,6,6,7,7,7-nonafluoroheptyl aspartate) block copolymer.

* Corresponding author. Tel.: +81 3 3433 1111x2336; fax: +81 3 3459 6005.
E-mail address: masajun2093ryo@jikei.ac.jp (M. Yokoyama).

0378-5173/$ – see front matter © 2011 Elsevier B.V. All rights reserved.
doi:10.1016/j.ijpharm.2011.10.006

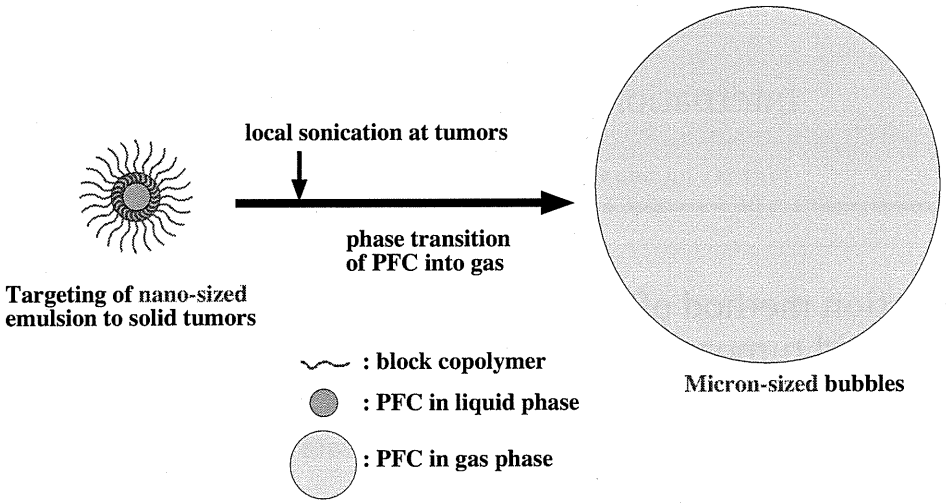

Fig. 1. Concept of phase-transition type nano-emulsion.

tumor theranostics. In order to resolve this dilemma, Kawabata et al. (Asami et al., 2009, 2010; Kawabata et al., 2005, 2010a,b) and Rapoport et al. (Mohan and Rapoport, 2010; Rapoport et al., 2007, 2009a, 2009b, 2010a,b, in press) examined nano-emulsions incorporating a specific kind of perfluorocarbon, as illustrated in Fig. 1. A boiling temperature of this perfluorocarbon (perfluoropentane, PFC5) is 29 °C, which is lower than normal human body temperature, but the integrity of these nano-emulsions is maintained owing to interfacial excessive pressure called Laplace pressure (Rapoport et al., 2009a). Upon ultrasound irradiation, the integrity of these nano-emulsions is broken, and this liquid perfluorocarbon exhibits a phase-transition into gas. Accordingly, the nano-emulsions change into microbubbles. Efficient delivery into tumor tissues is attained with the nano-emulsions, and then local sonication at the tumor tissues generates the microbubbles from the nano-emulsions, resulting in high imaging and therapeutic efficiencies. This phase-transition type nano-emulsion may be an ideal system for the theranostics of solid tumors.

Generally, preparations of smaller emulsions in a nano-meter range are more difficult because a higher power input is required in the emulsion preparations. (Tadros et al., 2004) Previously, we had prepared perfluorocarbon-containing emulsions by means of vigorous mechanical stirring with a magnetic stirrer and obtained emulsions of ca. 600 nm in diameter (Nishihara et al., 2009). In this paper, we have tried to obtain much smaller emulsions by means of ultrasound irradiation as well as high-pressure emulsification. Another important parameter for preparations of the phase-transition type nano-emulsion is temperature. A boiling temperature (29 °C) of perfluoropentane (PFC5) is close to the room temperature; therefore, preparations must be carried out at a low temperature and in a small scale for evasion of evaporation of PFC5 because heat generated in emulsification or sonication processes must be efficiently removed for the evasion. We want to find a facile preparation method that can be carried out at either room or a higher temperature, and that can be easily scaled up because the heat removal is a much less serious concern than the conventional method. Rapoport et al. (Rapoport et al., 2010b) reported preparations of nano-bubbles by means of ultrasound irradiation (with a probe type sonicator at 20 kHz) in ice-cold water. They obtained nano-emulsions of ca. 600 nm in diameter.

In this paper, we have tried to obtain very small nano-emulsions containing PFC5 by using an inexpensive bath-type sonicator (usually used as an ultrasonic cleaner) at room temperature or higher. For this emulsion preparation, we synthesized fluorinated block copolymers and optimized their compositions.

2. Materials and methods

2.1. Materials

We purchased perfluoropentane (PFC5) and perfluorohexane (PFC6) from Stream Chemicals (Newburyport, MA, USA) and Alfa Aesar (Ward Hill, MA, USA), respectively, and used them as received. We purchased 4,4,5,5,6,6,7,7,7-nonafluoroheptyl iodide from Sigma–Aldrich (Tokyo branch, Japan) and used it as received. We purchased reagent-grade solvents, dehydrated *N,N*-dimethylformamide (DMF), dimethyl sulfoxide (DMSO), and diethyl ether from Wako Chemicals (Tokyo, Japan), and used them as received. Poly(L-lactic acid)-grafted gelatin was prepared through a coupling reaction between a primary amine group of gelatin and a terminal hydroxyl group of the poly(L-lactic acid) by the use of disuccimidyl carbonate according to a published synthetic procedure. (Tanigo et al., 2010) Poly(ethylene glycol)-block-poly(L-lactic acid) block copolymer (PEG-b-PLA) was purchased from Sigma–Aldrich (Tokyo branch, Japan). The average molecular weights of the PEG block and the PLA block were 750 and 1,000, respectively.

2.2. Block copolymer synthesis

Poly(ethylene glycol)-*b*-poly(4,4,5,5,6,6,7,7,7-nonafluoroheptyl aspartate) block copolymers (PEG-P(Asp(C7F9)*x*)) were prepared by means of esterification of the aspartic units of poly(ethylene glycol)-b-poly(aspartic acid) block copolymer (PEG-P(Asp)) by the use of an iodinated compound, as shown in Fig. 2. PEG-P(Asp) was synthesized according to our previous paper (Yamamoto et al., 2007). A value *x* in the PEG-P(Asp(C7F9)*x*) formula denotes mol.% of the esterified units. This esterification reaction was carried out with a corresponding iodinated compound in the presence of a super base according to a previously reported procedure (Opanasopit et al., 2004; Yokoyama et al., 2004; Yamamoto et al., 2007) with a slight modification.

The starting material was poly(ethylene glycol)-b-poly(aspartic acid) block copolymer (PEG-P(Asp)). The average molecular weight of PEG was 5200 (n = 119 in Fig. 2), and the average number of Asp units per one chain was 26.0. The aspartate amide bond can be either α or β, and our group previously had reported that a ratio of α:β was 1:3 (=*a*:*b* in Fig. 2) (Yokoyama et al., 2004). PEG-P(Asp) (2.001 g, containing 6.33×10^{-3} mol Asp residue) was dissolved in 20 mL of DMF. To this mixture, was added both 4.904 g of 4,4,5,5,6,6,7,7,7-nonafluorohepty iodide (which is

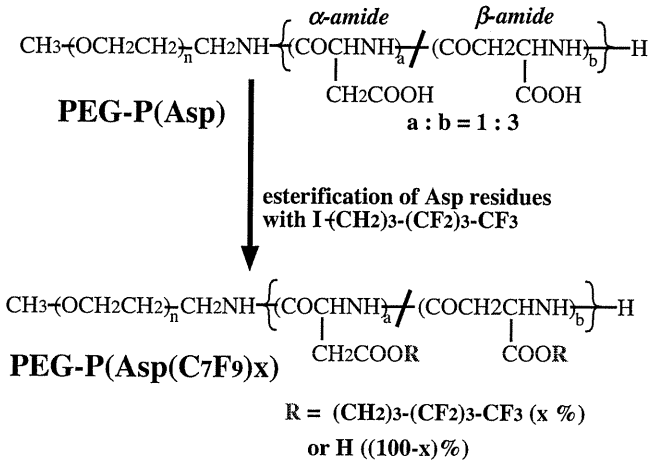

Fig. 2. Synthesis of the fluorocarbon-containing block copolymer PEG-P(Asp(C7F9)x).

2.00 mol. equivalents to the Asp residue, I-(CH2)3-(CF2)3-CF3 in Fig. 2) and 0.972 g of 1,8-diazabicyclo[5.4.0]undec-7-ene (DBU, which is 1.01 mol. equivalents to the Asp residue). DBU is a very strong base, and can induce ionization in a carboxyl group of the aspartic acid residue in an organic solvent, DMF. The reaction mixture was heated at 50 °C for 16 h. An ester formed at the Asp residue through a nucleophilic substitution reaction of the ionized carboxyl group with I-(CH2)3-(CF2)3-CF3. After this 16-h reaction, the reaction mixture was poured into 200 mL of ice-cold diethyl ether for precipitation of the polymer. The precipitated polymer was filtered and washed with diethyl ether. The obtained polymer was dissolved in 20 mL of DMSO, to which was added 2.11 mL of 6 N hydrochloric acid. This acid works for removal of DBU from polymers. This polymer solution was dialyzed with a Spectra/Por 6 dialysis membrane (molecular weight cut-off is 1000) against DMSO for 2 days and against milliQ water for an additional 2 days, followed by freeze-drying. Yield was 2.436 g. To determine the contents of the fluorinated ester group of the polymer, we used ^{1}H NMR spectroscopy in DMSO-d_6 containing 3 v/v% trifluoroacetic acid. For this determination, we identified a peak area ratio between the methylene protons ($-COOCH_2\underline{CH_2}CH_2CF_2CF_2CF_2CF_3$) at 1.8 ppm of the ester group and the methylene protons ($-OC\underline{H_2}C\underline{H_2}-$) at 3.6 ppm of the PEG block. The esterification percentage (x in Fig. 2) was revealed to be 59%. The other compositions of block copolymers were synthesized according to the same method with various molar ratios of I-(CH2)3-(CF2)3-CF3 and DBU with respect to the aspartic acid residue. Table 1 lists all the compositions of the synthesized block copolymers.

Table 1
Compositions of PEG-P(Asp(C7F9)x).

Code	M.W. of PEG	Asp unit number (n)	Esterification degree (x%)
F-6%	5200	22.1	5.9
F-15%	5200	23.3	14.6
F-39%	5200	22.1	38.5
F-59%	5200	26.0	58.5
F-67%	5200	22.1	67.0

2.3. Preparation of PFC-containing nano-emulsions

We examined preparations of PFC5-containing nano-emulsions according to two methods using a high-pressure emulsifier and a bath-type sonicator.

2.3.1. Preparation with a high-pressure emulsifier

We dissolved PEG-P(Asp(C7F9)15) block copolymer by stirring it in distilled water at a concentration of 4.0 wt. % of the solution, and added perfluoropentane (PFC5) and perfluorohexane (PFC6) at each 1.25 vol.% of the solution. We vigorously stirred the solution with a homogenizer Polytron (Kinematica AG, Tokyo, Japan) at 25,000 rpm for 10 s. Then, we conducted emulsification using a high-pressure emulsifier EmulsiFlex-C5 CSC (AVESTIN, Inc., Ottawa, Ontario, Canada) at 4 °C for 6 min at ca. 50 MPa. We collected a white emulsion, and filtered it with a Sartorius Minisart (R) filter (1.2 μm pore, Sartorius AG, Göttingen, Germany).

2.3.2. Preparation with a bath-type sonicator

We dissolved PEG-P(Asp(C7F9)x) block copolymers in MilliQ water at a concentration of 1.0 to 4.0 wt.% of water. In case of a high ester content such as x = 59, we heated (up to ca. 40 °C) and sonicated the solutions until we obtained a transparent polymer solution. The polymer solution was transferred to a 1.5-mL glass vial that was sealed with a Teflon–silicon rubber cap (Chromacol auto-sampler vial 2-SV for HPLC; GL Science, Inc., Tokyo, Japan), and was cooled on ice. Then, we added perfluoropentane (PFC5) and perfluorohexane (PFC6) at 0.5–4.0 vol.% of water. We confirmed PFCs' position at the bottom of the solution. (Sometimes PFCs, whose densities are much greater than water's, did not go into the aqueous solution. Therefore, we shook the vial vigorously to allow PFC droplets to sink to the bottom by force of gravity.) Then, we sealed the vial with a cap, and applied sonication for 3 min with a bath-type sonicator Branson model 1510 (oscillating frequency at 42 kHz, max. power intensity: 90 W, Danbury, CT, USA). The temperature of the bath was kept constant with degassed cold and hot water. In all the sonication procedures, we had a constant water level in a sonicator bath and a fixed position of the vial in order to obtain sonication conditions that were as identical to one another as possible. Finally, we collected a supernatant by leaving unincorporated PFC droplets at the bottom.

Table 2
Effects of polymer composition and sample volume on PFC5 incorporation behaviors.

Run	Polymer	Sample volume (μL)	PFC5 concentration (vol.%)[a]	Cumulant average diameter (nm)[a]
1	F-6%	300	0.840 ± 0.097	261.2 ± 3.4
2	F-15%	300	0.948 ± 0.131	232.4 ± 14.5
3	F-39%	300	0.625 ± 0.074	198.4 ± 33.3
4	F-59%	300	0.669[b]	133.9[b]
5	F-67%	300	0.682 ± 0.060	222.8 ± 37.9
6	F-59%	300	0.682 ± 0.074	205.5 ± 15.8
7	F-59%	300	0.634 ± 0.361	173.5 ± 24.5
8	F-59%	700	1.110[b]	231.8[b]
9	F-59%	1200	1.792[b]	280.6[b]

[a] Average ± standard deviation (n = 3) except runs 4, 8, and 9.
[b] Average of two preparations.

In order to measure amounts of the polymer chains that were not included in the PFC-emulsions, we carried out the following experiment. PFC-emulsion was prepared in the conditions of Run 4 of Table 2; polymer: F-59%, sample volume: 300 μL, polymer concentration: 4 wt.%, PFC5: 2 vol.%, PFC6: 2 vol.%, sonication at 40 °C for 3 min. The obtained emulsion was transferred into a 1.5 mL Eppendorf-type poly(propylene) tube and centrifuged at 13,200 rpm for 5 min with an Eppendorf centrifuge model 5415D (Eppendorf Co., Ltd. Japan, Tokyo, Japan). The emulsion was found to precipitate at the bottom. 200 μL of the supernatant was collected and freeze-dried. We calculated the polymer amounts that were not included in the PFC-emulsions by multiplying 1.5 (=300 μL/200 μL) to the freeze-dried polymer weight. As a control, we carried out the same experiment just only for the polymer (without addition of TFC5 nor TFC6).

2.4. Measurements

2.4.1. Dynamic light scattering (DLS)

The size of emulsions was measured with a dynamic light scattering (DLS) instrument, the DLS-7000 (Otsuka Electronics, Tokyo, Japan). DLS samples were prepared through appropriate dilution of the emulsions with commercial distilled water for internal injection (Otsuka Pharmaceutical Co. Ltd., Tokyo, Japan). The measurements were made at 25 °C, and scattering was observed at a 90° angle with respect to the incident beam. The cumulant average particle size and the particle size distribution from a non-negative least square method were determined by the use of software provided with the instrument.

2.4.2. Gas chromatography

We measured concentrations of PFC5 using two gas chromatograph systems as described below. In both cases, we successfully obtained clear separation of PFC5's peak from PFC6's peak, and carried out quantitative analyses using a standard sample of PFC5. Therefore, the two gas chromatograph systems gave us identical results. However, we only used the (2) system described below for blood samples because its pre-heating function was essential for measurements of blood samples.

2.4.2.1. Gas chromatograph system. We measured PFC5 using a gas chromatograph model G-6000 (Hitachi High-Technologies Corporation, Tokyo, Japan) equipped with a Gaskuropack 54 80/100 packed column (GL Sciences, Inc., Tokyo, Japan) and an FID detector at 200 °C. Carrier gas was nitrogen at a flow rate of 300 mL/min. 5 μL of a sample solution were injected into the gas chromatograph system with a micro syringe at 0 min. Column temperature was controlled in the following manner; 100 °C (0 min), raised at a rate of 5 °C/min until 130 °C (6 min), and then raised at a rate of 60 °C/min until 190 °C (7 min), followed by maintenance of 190 °C for 2 min. PFC5 and PFC6 were found to elute at 3.8 min and 6.4 min, respectively.

2.4.2.2. Gas chromatograph system. We measured PFC5 using a gas chromatograph system GC-2014 (Shimadzu Corp., Kyoto, Japan) equipped with an FID detector at 250 °C. We used two tandem-connected two columns: DB-WAX 127-7012 (Agilent Technologies Japan, Ltd., Tokyo, Japan) and RESTEK Rt-QBond 19741 (Shimadzu GLC Ltd., Tokyo, Japan). Carrier gas was helium at a flow rate of 20 mL/min. Either 100 or 544 μL of a sample solution were heated at 200 °C and injected with a headspace autosampler TurboMatrix Trap 40 (PerkinElmer Japan Co., Ltd., Yokohama, Japan). Column temperature was constant at 150 °C. PFC5 and PFC6 were found to elute at 3.6 min and 4.4 min, respectively.

2.5. Measurements of PFC5 concentration in blood

In vivo PFC5 concentration profiles in blood were evaluated in Balb/c female mice (6 weeks old). 100 μL of PFC-emulsion was intravenously administered via lateral tail veins. The emulsions' PFC5 concentrations ranged from 0.429 to 0.670 vol.%. Blood (44 μL) was collected with a heparinized blood-collecting glass tube, and mixed with 500 μL of heparin solution in a capped sample tube of the (2) gas chromatograph system.

3. Results

3.1. General characteristics of the emulsion-preparation method with a bath-type sonicator

In representative conditions, we successfully obtained PFC5-containing nano-sized emulsions having diameters of ca. 200 nm in considerably high PFC5 yields. Fig. 3(a) and (b) shows diameter distributions measured by means of dynamic light scattering (DLS) for PEG-P(Asp(C7F9)59) (F-59% in Table 1). In these conditions, we dissolved 12.0 mg of polymer in 300 μL water (4.0 wt.% solution), and put this polymer solution in a 1.5 mL glass vial, followed by additions of 6 μL (corresponding to 2.0 vol.% of water) of PFC5 and 6 μL of PFC6. Sonication was performed for 3 min in a bath-type sonicator at 40 °C. In the first three preparations (run 6 in Table 2), the cumulant diameter obtained was 205.5 ± 15.8 nm (the average ± standard deviation; $n = 3$), and Fig. 3(a) shows the weight-weighted diameter distribution of one preparation. Almost uniformly distributed emulsions were obtained, and the diameter of the emulsion droplets had a very small size about 200 nm. In this run 6, PFC5 concentrations were 0.682 ± 0.074 vol.%. These values are considered large enough for ultrasound images (Kawabata et al., 2005, 2010a,b). In another set of three preparations (on another day, run 7 in Table 2), we obtained a very similar average diameter, 173.5 ± 24.5 nm (the average ± standard deviation; $n = 3$) and PFC5 concentrations. The diameter distribution of one preparation of run 7 is shown in Fig. 3(b). These two figures exhibited a major peak at about 200 nm, while a minor peak was seen in a larger diameter side and a smaller diameter side, as shown in Fig. 3(a) and (b), respectively. This difference may result from a slight variation in sonication conditions such as the position of samples and the water level of the sonicator. These emulsions were obtained and measured without any purification process after the sonication, and a large majority of the emulsions in weight were found to have a diameter of about 200 nm. All these results clearly indicate that this sonication method brought about very small nanometer-sized PFC5-containing emulsions with considerably high PFC5 concentrations.

We measured a proportion of polymer incorporated in the PFC-emulsion out of the feed polymer amount. In these preparation conditions (run 7 in Table 2), 75.4 ± 2.6% ($n = 3$) of the feed polymer was found in a supernatant obtained after centrifugation. (All the PFC-emulsions were observed to precipitate in this centrifugation.) When this measurement was carried out for the polymer alone, 93.8 ± 2.0% ($n = 3$) of the feed polymer was found in a supernatant obtained after centrifugation. Therefore, 18.4% (=93.8%–75.4%) of the feed polymer was considered to be incorporated into the PFC-emulsions. Removal of the free polymer chain, that was not incorporated into the PFC-emulsion, was not examined in this study. The removal is difficult because the free polymer existed as a polymeric micelle was close to the PFC-emulsion in size. (If the free polymer existed as a single polymer chain, a difference in size between the free polymer and the PFC-emulsion would be so large to allow separation such as ultrafiltration.)

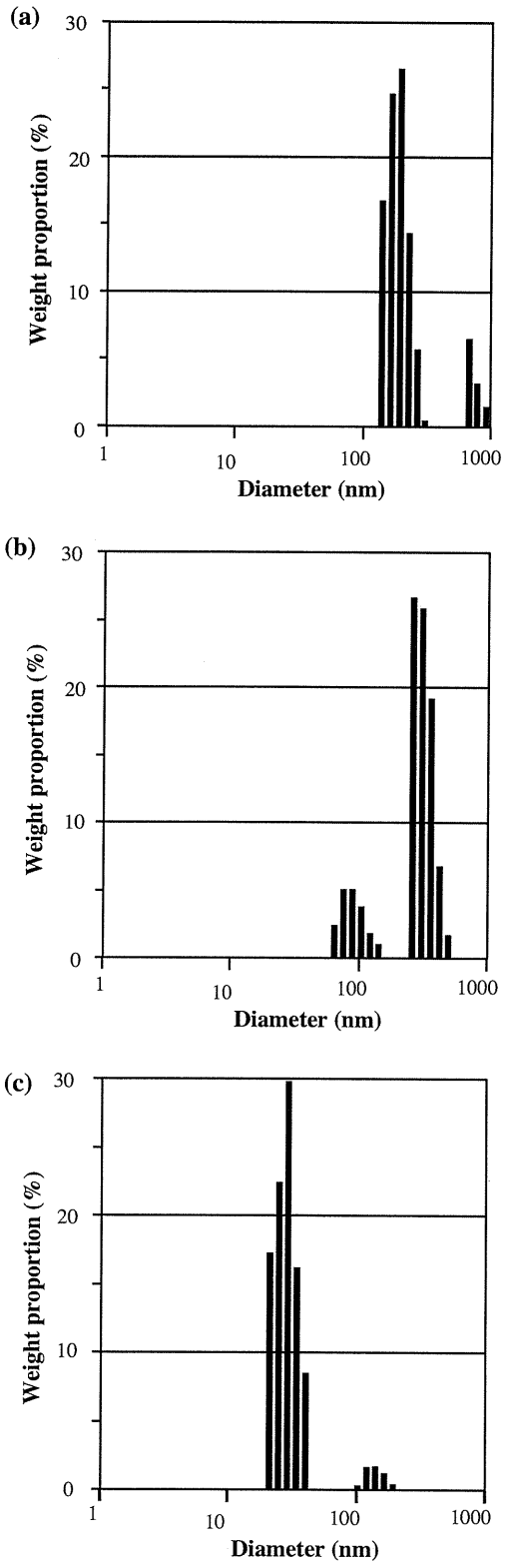

Fig. 3. Diameter distribution of PFC5-containing nano-emulsions (a and b) forming from PEG-P(Asp(C7F9)59) and empty polymeric micelle (c) measured by means of DLS. (a and b) are of different batches but prepared in the same conditions.

Using this polymer amount incorporated into the PFC-emulsions, we calculated the thickness of the polymer shell. We carried out the calculation with the following assumptions.

(1) The PFC-emulsions are made of the two phases; the inner PFC droplet phase and the outer polymer shell phase.
(2) We obtained PFC6 amounts in the emulsions assuming that sensitivity of PFC6 in gas chromatography is the same as that of PFC5. (The same peak area per PFC volume.)
(3) PFC6 and PFC5 are mixed freely without any gain or loss of droplet volume.
(4) Density of polymer is 1.03. (This is a common value of protein, and most synthetic polymers show similar values.)

The obtained value of the polymer shell's thickness was 22 nm, while the radius of the PFC droplet was 65 nm. In the future study, we like to analyse relationships between the shell thickness and physical stability of the emulsions.

3.2. Comparison with other emulsion-preparation methods

We compared the PFC5's concentrations of the PFC5-containing emulsions prepared in the sonication method with the PFC5's concentrations of the emulsions prepared in two common methods; mechanical stirring and high-pressure emulsification (Solans et al., 2005). We also compared the diameters of the emulsions prepared in the sonication method with those prepared in the two common methods. Previously, we reported PFC5-containing emulsions prepared by means of mechanical stirring that featured a magnetic stirrer (Nishihara et al., 2009). In this method, only the F-14% polymer provided a high PFC5 concentration (0.65 vol.%). The other polymers provided low or very low PFC5 concentrations: F-6% had 0.28 vol.%, F-22% had 0.19 vol.%, F-39% had 0.02 vol.%, and F-67% had 0.01 vol.%. In the F-14% case, the cumulant diameter was 694 nm, which was much larger than those obtained in the sonication method as described in the previous section (Section 3.1). Another distinct difference was found in a wide range of polymer compositions for high PFC5 concentrations in the sonication method. As summarized in runs 1–5 of Table 2, we compared the PFC5 concentrations (vol.%) and average diameters of the PFC5-containing emulsions for five polymer compositions. All these five compositions of polymers provided high PFC5 concentrations larger than 0.6 vol.%. Furthermore, all emulsion sizes of these runs (runs 2–5) were revealed to be small, at about 200 nm.

In the next step, we compared the sonication method with the most common method for emulsion preparation:high-pressure emulsification. For this comparison, we used F-15% polymer. We compared PFC5 concentrations and the cumulant average diameters of the emulsions prepared in the sonication method with PFC5 concentrations and the cumulant average diameters of the "high-pressure method" emulsions. We acquired a considerably high PFC5 concentration, 0.58 vol.%, by using a high-pressure emulsifier for the high-pressure emulsification method (its procedure is described in Section 2.3.1). However, the cumulant average diameter of the obtained emulsion was 477 nm. This value was much larger than the sonication-method value (232.4 nm, run 2 of Table 2). Additionally, maintenance of a low temperature at 4 °C for the whole instrument was essential in the high-pressure emulsification method, since possible heat generation due to the high-pressure process may considerably boost evaporation of PFC5 (the boiling temperature of PFC5 is 29 °C). In contrast, in the sonication method, a high PFC5 concentration was obtained at 40 °C, which is above PFC5's boiling temperature. (The temperature issue of the emulsion-preparation process will be more closely examined in the following section (Section 3.4).)